

June 2021

PhD Dissertation

Evolutionary Synthesis of Reliable Digital Circuits

Graduate School of Chosun University

Department of Computer Engineering

Umar Afzaal

Evolutionary Synthesis of Reliable Digital Circuits

진화기반 신뢰성 높은 회로 합성 연구

August 27, 2021

Graduate School of Chosun University

Department of Computer Engineering

Umar Afzaal

Evolutionary Synthesis of Reliable Digital Circuits

Advisor: Lee, Jeong-A

A dissertation submitted in partial fulfillment of the requirements for a
Doctoral Degree

April 2021

Graduate School of Chosun University

Department of Computer Engineering

Umar Afzaal

This is only a sample. You will get approvals from your committee members after a successful thesis defense

아프잘 우마 박사학위논문을 인준함

위원장 조선대학교 교수 모상만



위원 조선대학교 교수 신석주



위원 조선대학교 교수 정호엽



위원 한림대학교 교수 이정근



위원 조선대학교 교수 이정아



2021년 06월 30

조선대학교 대학원

Dedicated to parents who love unconditionally.

ACKNOWLEDGEMENTS

All praise is due to the Lord of the Worlds alone. This thesis made possible, my heartfelt regard for the constant reassurance and prayer of my parents who words cannot describe the level of patience with which they persevere my absence. The exceptional guidance and support from Professor Lee, my supervisor during the course of this degree. In sincere acknowledgment, the outstanding companionship of the Muslim community, and in gratefulness, especially the generous hospitality, Mr. Muhammad Adnan, Miss Zobia Irshad, Mr. Zahid Hussain, Mr. Abdus Sami Hassan and Mr. Usman Afzaal. Thank you everyone.

TABLE OF CONTENTS

| | |
|--|-------------|
| LIST OF ABBREVIATIONS AND ACRONYMS | v |
| LIST OF FIGURES | vi |
| LIST OF TABLES | viii |
| ABSTRACT | ix |
| 한 글 요 약 | x |
| 1 INTRODUCTION | 1 |
| 1.1 Hexagonal Boron Nitride and Graphene | 1 |
| 1.2 2D Materials-based Metal Matrix Composites | 4 |
| 1.3 Current Challenges for Fabricating 2D Materials-Based MMCs | 6 |
| 1.4 Fabrication Methods | 8 |
| 1.4.1 Mechanical Alloying (MA) | 8 |
| 1.4.2 Semi Powder Metallurgy (SPM) | 9 |
| 1.4.3 Molecular-level Mixing (MLM) | 10 |
| 1.4.4 In-situ Growth | 11 |
| 1.5 Applications of Gr/hBN in MMCs | 14 |
| 1.5.1 Mechanical Properties | 14 |
| 1.5.1.1 Load Transfer | 14 |
| 1.5.1.2 Dislocation Strengthening | 15 |
| 1.5.1.3 Grain refinement | 16 |
| 1.5.2 Thermal properties | 16 |
| 1.5.3 Corrosion Properties | 17 |
| 1.6 Summary | 18 |

| | | |
|---|--|-----------|
| 2 | Synthesis of Three-Dimensionally Interconnected Hexagonal Boron Nitride Networked Cu-Ni Composite | 19 |
| 2.1 | Introduction | 19 |
| 2.2 | Fabrication of 3Di-hBN CuNi Composite | 21 |
| 2.2.1 | Compaction of CuNi powders | 21 |
| 2.2.2 | Metal Organic Chemical Vapor Deposition | 22 |
| 2.3 | Characterization of 3Di hBN-CuNi Composites | 25 |
| 2.3.1 | Green and Composite Density | 25 |
| 2.3.2 | Microstructural Characterization | 25 |
| 2.3.3 | Mechanism of hBN Formation at Grain Boundaries | 26 |
| 2.4 | Optimal Conditions of Constructing 3Di-hBN in 3Di hBN-CuNi composite | 27 |
| 2.5 | Microstructural Investigation | 30 |
| 3 | SUMMARY AND CONCLUSIONS | 34 |
| PUBLICATIONS | | 35 |
| BIBLIOGRAPHY | | |
| APPENDIX A: Main Reagents and Materials | | |
| APPENDIX B: Synthesis and Characterization Tools | | |
| B.1 | CVD System | |
| B.1.1 | Pneumatic Control and Vacuum System | |
| B.2 | Other Experimental Instruments | |
| B.3 | Characterization Methods | |

LIST OF ABBREVIATIONS AND ACRONYMS

| | |
|-------------|---|
| CMOS | Complementary metal–oxide–semiconductor |
| SEU | Single-event upset |
| SET | Single-event transient |
| PO | Primary output |
| TMR | Triple modular redundancy |
| ATMR | Approximate triple modular redundancy |
| FATMR | Full approximate triple modular redundancy |
| DWC | Duplication with comparison |
| TSC | Totally self-checking circuits |
| CED | Concurrent error detection |
| SOP | Sum of products |
| POS | Products of sum |
| FPGA | Field-programmable gate arrays |
| FMR | Fault masking ratio |
| P_{fault} | Fault-observation probability |
| CLB | Configurable logic blocks |
| PE | Processing element |
| LUT | Look-up table |
| CNN | Convolutional neural network |
| CGP | Cartesian genetic programming |
| CS | Cuckoo search |
| CS-GRN | Cuckoo search with genetic replacement of abandoned nests |
| CNF | Conjunctive normal form |
| SAT | Satisfiability |
| PDP | Power-delay product |
| EP | Error probability |

LIST OF FIGURES

| | |
|---|----|
| 1.1 Schematic illustration of the in-situ growth for graphene reinforced Cu composite (Guo et al., 2020). | 12 |
| 1.2 Schematic diagrams (a) 3DiGr (black areas) in Gr-Cu composite transferring the load in matrix(Chu et al., 2018b) (b)Section view of graphene/Cu in the fracture process, the graphene delays the fracture under the mechanism of load transfer (Chen et al., 2016). | 15 |
| 2.1 Mold and hydraulic press used for powder compaction. | 22 |
| 2.2 Cu and Ni particles shown at the fracture surface of the disc after compaction. | 23 |
| 2.3 (a) Schematic illustration of the fabrication of 3Di-hBN-Cu-Ni composite and (b) disc-shaped 3Di-hBN-Cu-Ni composite fabricated using a simple two-step process. | 24 |
| 2.4 Schematic showing the process of formation of 3Di-hBN-Cu-Ni composite. | 27 |
| 2.5 OM images of 3Di-hBN-Cu-Ni composites under various conditions. | 28 |
| 2.6 Density of the 3Di-hBN-Cu-Ni composite as a function of compacting pressure and sintering time. | 29 |
| 2.7 OM images of 3Di hBN-Cu-Ni composites processed at compaction pressures of (a) 280 MPa and (b) 335 MPa. | 29 |
| 2.8 SEM image showing the surface morphology of the 3Di-hBN-Cu-Ni composite fabricated with compaction pressure of 280 MPa and sintering time of 30 min. | 31 |
| 2.9 SEM image showing the 3D interconnected network of hBN in 3Di hBN-Cu-Ni composite produced under compaction pressure of 280 MPa and sintering time of 30 min, respectively. | 32 |
| 2.10 (a) XRD pattern of 3Di-hBN-Cu-Ni composite and (b) Elemental distribution map of 3Di-hBN-Cu-Ni composite. | 32 |

| | |
|--|----|
| 2.11 TEM investigation: (a) low-magnification bright-field TEM image of 3Di-hBN; (b) HR-TEM image showing 2–6 layers of hBN; inset shows a distance of 0.25 nm between layers. | 33 |
|--|----|

LIST OF TABLES

| | | |
|-----|--|----|
| 1.1 | Mechanical properties of graphene reinforced MMCs. | 14 |
| 1.2 | Thermal conductivities of graphene reinforced MMCs. | 17 |
| 2.1 | Chemical compositions of Cu and Ni powders. | 22 |
| 2.2 | EDS results of the 3Di-hBN-Cu-Ni composite for the microstructure shown in Figure 2.8. | 30 |
| A.1 | Main Reagents and Materials. | |
| B.1 | Instruments and their usage. | |
| B.2 | Instruments and their usage. | |

ABSTRACT

Evolutionary Synthesis of Reliable Digital Circuits

Umar Afzaal

Advisor: Prof. Lee, Jeong A

Department of Computer Engineering

Graduate School of Chosun University

In the event of an upset, fault-resilient circuits maintain correct functionality allowing the system to remain fully operational or at least operate with a graceful degradation. Every circuit has a certain level of inherent resilience to faults. Often times, this inherent resilience to faults is insufficient for the given application. This is because conventional synthesis tools generally only focus on optimizing a circuit with respect to area, power or timing budgets. There is a wide range of applications where faulty circuit behavior can lead to fatal results. Fault injection analyses are reported and show that even a single fault can be critical to the desired circuit operation in such applications.

To which end, in this thesis, we present SYFR, an evolutionary method for automated synthesis of increased fault-resilience digital circuits suitable for fine-grained use. Tests results for synthesis of up to 60 input circuits with SYFR are reported. SYFR can be repeatedly applied to a circuit to obtain various design tradeoffs between fault- resilience and implementation costs. SYFR can also be flexibly applied to build circuits which are selectively fault-resilient, i.e., their tolerance to faults is workload-aware. In addition, a novel population seeding mechanism to reduce the design space is introduced and experimentally validated.

In summary, it is shown that SYFR can be considered a competitive synthesis methodology for constructing fault-resilient circuits.

한글 요약

진화기반 신뢰성 높은 회로 합성 연구

아프잘 우마

지도 교수: 이정아

컴퓨터공학과

대학원, 조선대학교

신뢰성 높은 회로는, 오류가 발생한 경우에도 회로의 올바른 기능을 유지하여 시스템이 정상적인 작동 상태를 유지하거나 최소한의 단계별 오류 조치로 작동할 수 있게 한다. 모든 회로에는 회로 고유의 오류 허용 내결함성이 있다. 그러나 이러한 오류에 대한 회로 고유의 복원력은 주어진 응용분야에 대부분 충분하지 않다. 이는 기존 회로 합성 도구가 면적, 전력소모, 실행시간을 고려한 회로 최적화에 초점을 일반적으로 맞추고 있기 때문이다. 오류에 의한 회로 동작이 치명적인 결과로 이어질 수 있는 응용 분야는 다양하다. 이러한 응용분야에서는, 오류 모사 입력에 의한 분석을 통하여, 하나의 오류인 경우에도 회로 작동에 매우 심각한 영향을 끼칠 수 있음을 보일 수 있다.

본 논문에서, 신뢰성 높은 회로를 자동적으로 합성하는 방법론으로, 소규모 단위의 로직 변환을 고려하는 진화 기반의 SYFR (SYnthesis of Fault-Resilient circuits) 방법론을 제안한다. 본 방법을 이용하여 신뢰성 높은 회로를 직접적으로 합성한 결과는 60 개까지의 로직 입력을 가질 수 있음을 보였다. SYFR 기법은, 분할된 회로에 반복적으로 적용하는 방식을 통하여, 대형 회로에 적용할 수 있는데, 회로의 신뢰도와 회로 구현 비용 조율을 통하여 다양한 설계공간 탐색이 가능하다. 그리고, SYFR 방법론은 오류 발생시 고장 복원력이 있는, 신뢰성 높은 설계 회로 합성에 워크로드 기반으로 선택적으로 유연하게 적용할 수 있다. 본 논문에서 신뢰성 높은 회로의 설계 공간을 줄이기 위한 모집단 씨앗 메커니즘을 새롭게 제안하였으며, 실험결과로 이의 효용성을 보였다. 본 논문은 SYFR 방법론이 신뢰성 높은 회로를 합성하기 위한 경쟁력 있는 방법론으로 간주될 수 있음을 보여준다.

1 INTRODUCTION

1.1 Hexagonal Boron Nitride and Graphene

Since the successful isolation of graphene from graphite by the Scotch tape method reported by Novoselov and Geim in 2004 (Novoselov et al., 2004) the research on graphene and two-dimensional (2D) materials has been exploded due to their unique, peculiar and fascinating low dimensional structures and properties in contrast to those of their bulk and other dimensional counterparts (Xu et al., 2013). In the past few years, tremendous attention has been paid to 2D hexagonal boron nitride (hBN), which is by itself an electrical insulator with an ultra-flat surface and a highly stable structure. Although hBN is electrically insulating, it can well be tuned by several strategies for differing properties and functionalities, such as by doping, substitution, functionalization and hybridization (Zhang et al., 2017a). It can also be used to tune the carrier mobility of other two-dimensional materials, such as graphene, MoS₂ and BP, when properly synergized together due to the reduced coulomb scattering and excellent interface properties, and to protect these active materials from contamination, oxidation, and thermally/ electrically induced degradation (Zhang et al., 2017a). Driven by the anticipated huge technical potential, single- and few-layer hBN nanosheets have been successfully developed and investigated, which have indeed been shown to exhibit abundant appealing properties for technologically demanding applications, such as DUV photonic devices (Jiang and Lin, 2014) dielectric tunneling (Hui et al., 2016), power devices (Constantinescu and Hine, 2016), electronic packaging (Bao et al., 2016b), fuel cells (Oh et al., 2014), and biomedicines (Chimene, Alge, and Gaharwar, 2015). 2D-hBN nanosheets, which are sp²-hybridized 2D insulators, are structural analogues of graphene with sublattices being occupied by equal numbers of boron and nitrogen atoms alternately arranged in a honeycomb configuration. The hexagonal crystal structure of hBN with crystallographic parameters of $a = 0.250$ nm and $c = 0.666$ nm and the interlayer spacing of 0.333 nm enable excellent interaction with graphene, and hence it has great potential

for various device applications. Similar to graphene, the weak van der Waals interaction dominates between the different hBN planes, which are covalent-bonded within the plane and are highly polarized because of the high asymmetry of the sublattices, resulting in a large band gap (5–6 eV). As the weak interlayer interaction in hBN, van der Waals forces and electrostatic forces are largely responsible for anchoring the interlayer distance and dictating the optimal stacking modes.

The characteristic resistance to oxidation and corrosion makes 2D-hBN a suitable candidate as a gate dielectric and capping layer to protect the active material element and device from structural deformation and chemical degradation (Li and Chen, 2016). Additionally, due to being electrically insulative with a wide bandgap of 5.97 eV and optically transparent, 2D-hBN can be applied as a barrier and active layer to implement the tunneling devices and tune the carrier dynamics and optical properties. Its high thermal stability (up to 1000 °C in air and 1400 °C in vacuum) (Li et al., 2014a), superior thermal expansion coefficient (1-layer, 2-layer and 9-layer correspond to 3.41 10², 3.15 10² and 3.78 10² cm⁻¹ K⁻¹, respectively) and conductivity (484 W m⁻¹ K⁻¹) as well as excellent mechanical strength (elastic constant of 220–510 Nm⁻¹ and Young's modulus 1.0 TPa) (Kumar, Rajasekaran, and Parashar, 2016; Wang et al., 2016) further benefit 2D-hBN in various other applications. The stability and performance of 2D-hBN-based devices are of course highly dependent on the quality of 2D nanosheets, which consequently requires a careful control of the synthesis process. This has indeed stimulated new strategies and innovation in controlling the material growth processes and understanding the formation mechanisms (Wang et al., 2016; Bao et al., 2016a). Despite the great progress achieved so far, the current research into 2D-hBN still faces three major challenges: (a) growth of large-scale hBN with controlled layer quality and corresponding transfer technique, (b) integration of 2D-hBN into other nano-materials or nano-devices, (c) effective modulation of electronic structures by other strategies (including energy bands and charge carriers) in 2D-hBN (Nam et al., 2014). Graphene is

a single layer of carbon atoms that are connected in hexagonal lattice to form honey comb structure. Thanks to its excellent thermal, mechanical, structural and optical properties (Lee et al., 2008; Calizo et al., 2009; Ahn et al., 2014; Balandin et al., 2008), graphene has gained a huge attention of research scientists. These outstanding properties are shown by graphene because of its unique electronic structure and hexagonal arrangement of carbon atoms in lattice (Neto, Guinea, and Peres, 2006). Graphene could be combined with other materials to synthesize graphene reinforced metal matrix composites (Gr-MMCs). Such composites take the benefit of extraordinary properties of graphene and, therefore, also exhibit excellent properties.

Carbon atom has electronic configuration of $1s^2\ 2s^2\ 2p^2$. When two carbon atoms combine together, sp^2 hybridization occurs because one election from 2s orbital transfers to 2p-orbital thereby bringing three orbitals 2s, 2px and 2py to same energy level (Littlejohn, 2013). This enables single carbon to form strong covalent bond with three carbon atoms thus forming a hexagonal lattice (Tiwari et al., 2016). The C-C planar sigma bond has bond length of 0.142 nm imparts graphene exceptionally high planar strength (Huang et al., 2011). Excellent functional properties of graphene are imparted by unhybridized 2pz orbitals which form delocalized electronic clouds over the hexagonal ring (Agarwal, Lahiri, and Bakshi, 2018). Due to unique atomic structure and electronic interactions, Dirac cones are formed at each edge of hexagonal ring. Graphene has zero bandgap nature because of these Dirac cones (Abbott's, 2007). High charge carrier mobility of graphene results in its excellent thermal and electrical conductivities because of the presence of massless Dirac fermions and ballistic charge transport (Bolotin et al., 2008). As mentioned earlier, the properties of graphene depend on the structure of carbon lattice and functional groups associated with each of its derivatives. Graphene derivatives can be classified into several types based on layers number, functional groups and crystallographic structure (Geim, 2009). On the basis of number of layers, the graphene derivatives are categorized into single-layer graphene, few layered graphene (FLG),

multilayered graphene (MLG), and graphene/graphite nanoplatelets (GNPs) (Kauling et al., 2018). In addition, graphene has excellent mechanical properties; the tensile strength of graphene measured by the experiment is about 130 GPa (lee2008measurement), which is 100 times that of ordinary steel; its fracture strength can reach 42 N/m^2 , about 200 times that of steel (lee2008measurement). At the same time, the elastic elongation of graphene is also higher than that of all other crystals, and the elongation rate can reach 20%; the elastic constant of graphene is $1 - 5 \text{ Nm}^{-1}$, and the Young's modulus is as high as 1.02 TPa (Lee et al., 2008). These excellent properties of graphene materials generated huge interests in the applying it in a myriad of device and in the fields of thermoelectric and optoelectronic devices, ultrastrong paper-like materials, electrocatalysts, novel composite materials, energy conversation materials, and so on. In this dissertation, the potential of graphene to reinforce metals and alloys will be focused.

Graphene and hBN materials hold a prominent position among nanomaterials due to their colossal potential to improve the properties of metals and alloys [xxx]. In order to benefit from their atypical functional and structural properties, scientific community continues to research on developing MMCs reinforced by graphene and hBN [xxxx]. Despite of all the research that has been performed on this topic, there are still some gaps which need to be filled and true potential of graphene or other 2D materials is yet to be explored. The fabrication techniques to develop 2D reinforced metal matrix composites (MMCs) are continuously flourishing; efficient and economical methods need to be introduced for the fabrication of 2D materials reinforced MMCs.

1.2 2D Materials-based Metal Matrix Composites

Metal-matrix composites are metals or alloys that incorporate particles, whiskers, fibers, or hollow micro balloons made of a different material, and offer unique opportunities to tailor materials to specific design needs (Mortensen and Llorca, 2010; Sidhu, Kumar, and Batish, 2016; Miracle, 2005). These materials can be tailored to be lightweight

and with various other properties including: high specific strength and specific stiffness, high hardness and wear resistance, low coefficients of friction and thermal expansion, high thermal conductivity, and high energy absorption and a damping capacity (Miracle, 2005). In addition to these properties, new MMCs are being developed with self-healing, self-cleaning, and self-lubricating properties, which can be used to enhance energy efficiency and reliability of automotive systems and components (Macke, Schultz, and Rohatgi, 2012). Since the last three decades, metal matrix composites (MMCs) have been intensively studied in order to develop high performance materials exhibiting distinguished properties.

MMCs can be divided into three different types in terms of the reinforcement, which are fibre-, particle- and flake-reinforced MMC (ClyneTW, 1993; Ibrahim, Mohamed, and Lavernia, 1991; Chawla, 2012). Fibre-MMC consists of reinforcement fibres and metal bulk in which the typical fibres are boron, SiC, Al₂O₃ and graphite (Chou, Kelly, and Okura, 1985). The reinforcement fibres are used for adhesion, stress transfer and thus effectively improve the tensile strength of the composites (Shirvanimoghaddam et al., 2017). The fibre-reinforced MMCs are usually used as structural materials with high strength and elastic modulus (Vijayaram et al., 2006). The particles used in particle-MMC are typically SiC, MoS₂ and h-BN particles (Chawla and Shen, 2001). These composites have less tensile strength and elastic modulus, while the hardness and stiffness are higher compared with fibre-MMC (Zhang, Zhang, and Mai, 1995). Therefore, particle-MMC is often used to enhance the tribological properties of composites (Chawla and Shen, 2001). As for flake-MMC, graphene is the most representative reinforcement component (Wang et al., 2012). With the aid of the excellent mechanical properties and unique pristine 2D structure of graphene, the tensile strength and elastic modulus could be extensively increased in two directions, other than the one-direction case of fibre reinforcement (Kumar and Xavior, 2014).

The performance of MMC mainly depends on the selection of reinforcement

materials for improving the mechanical and tribological properties (HG and Xavior, 2017). In the case of traditional MMC materials, the reinforcement materials include microparticles, fibres and crystal whiskers (Chawla and Shen, 2001). The recent development of 2D materials, including graphene, MoS₂, WS₂ and h-BN, which have naturally high strength and strong interfacial bonding, leads to the opportunity for tailoring the MMC materials in nanometre-scaled range with improved performance (HG and Xavior, 2017; Kasar, Xiong, and Menezes, 2018; Nieto et al., 2017; Nautiyal et al., 2019; Xiao et al., 2017). Many studies on these composites specifically address the uniform distribution problem of these 2D materials in a metal matrix, followed by the presence of porosity (HG and Xavior, 2017; Kasar, Xiong, and Menezes, 2018). On the other hand, the huge density difference between 2D materials and metal matrix, high interfacial contact area, and reaction activity of 2D materials will also lead to poor interfacial bonding between these 2D materials and metal matrix (Kasar, Xiong, and Menezes, 2018; Takeda et al., 2017). Therefore, it is essential to improve the dispersion properties of graphene, MoS₂, WS₂ and h-BN in metal matrix systems for enhanced mechanical properties of MMC. This review will first summarize the fabrication methods of MMC and the challenges in the fabrication process thus far. The effects of the reinforcement component on mechanical properties of MMC were presented, followed by the analysis of their mechanical and tribological properties.

1.3 Current Challenges for Fabricating 2D Materials-Based MMCs

Proper dispersion of graphene/hBN in a metal matrix is essential to achieve MMCs with desired properties. The incorporation of graphene/hBN should be carried out such that there is no agglomeration, uniform distribution, good interfacial attachment, and proper structural integrity. Severe agglomeration of graphene is one of the main problems to fabricate graphene reinforced metal matrix composites (Gr-MMCs) (Hu et al., 2016b). Agglomeration occurs as a result of Van der Waal's forces between

graphene sheets (Zandiatashbar, Picu, and Koratkar, 2012). Commonly, Gr-MMCs are fabricated using GNPs and MLGs which contain 10–100 layers of carbon atoms (Nieto et al., 2017). As a result, there is a big difference in properties between these multilayer graphene derivatives and a single layer graphene. With the multilayer graphene derivatives, agglomeration is one of the basic challenges because this can unavoidably lead to the large porosity in structure. This may in turn cause premature failure of the composite because of premature crack initiation and propagation (Song et al., 2016; Chu and Jia, 2014; Li et al., 2014b). Another serious concern is the poor dispersion of graphene in metal matrix (Chu et al., 2018a) which leads to the poor properties of MMCs. Inhomogeneous distribution of graphene results in increase in porosity and decrease in yield strength, thermal, and electrical conductivities of composite (Asgharzadeh and Sedigh, 2017). Furthermore, in order to ensure good properties of MMCs, wettability between the reinforcement material and metal matrix is also an important parameter to consider. If the wettability is low, there is weak interface between enforcement material and metal matrix and hence composite will demonstrate poor properties (Kauling et al., 2018). As mentioned earlier, graphene possesses extraordinary properties only due to its unparalleled electronic and chemical structure. So, in order to avail maximum benefits from the outstanding properties of graphene in MMCs, it is important that its chemical and electronic nature of structure is preserved. Unfortunately, conventional methods of fabricating MMCs impose harsh processing conditions and hence cause damaging the actual properties of graphene. Various types of deteriorations include thermal decomposition of graphene, high defect density in graphene sheets and lateral size reduction etc. (Nieto, Lahiri, and Agarwal, 2012; Pérez-Bustamante et al., 2014). These defects not only miserably affect the thermal and electrical behavior of MMCs but also result in premature failure (Chu et al., 2018c). It must be noted here that the hBN is structurally analogous to graphene having almost all comparable properties to graphene. In this perspective, the challenges towards the development of hBN reinforced

metal matrix composites (hBN-MMCs) are the same as towards the development of Gr-MMCs. In the coming section, we therefore present various processing techniques to fabricate Gr-MMCs with their advantages and limitations.

1.4 Fabrication Methods

Incorporation of graphene in metal matrices has been carried out by utilizing various techniques since last decade (Nieto, Lahiri, and Agarwal, 2012; Hu et al., 2016a; Kumar and Xavior, 2014). The main focus was to address the aforementioned challenges in the fabrication of Gr-MMCs. The processing techniques can be broadly classified into following classes.

1. Mechanical alloying (MA)
2. Semi powder metallurgy (SPM)
3. Molecular-level mixing (MLM)
4. In-situ growth

The forthcoming section illustrates an overview of each processing technique so that we could get familiarization about their scope.

1.4.1 Mechanical Alloying (MA)

MA involves the mixing and blending of graphene and metal powders. This technique is widely being employed for fabrication of Gr-MMCs (Kim, Lee, and Han, 2014; Dutkiewicz et al., 2015; Borkar et al., 2015; Yalçın et al., 2019; Salvo et al., 2019). Mixing and blending are mostly carried out by using ball milling technique which not only blends the graphene and metallic particles but also controls the morphology of metallic powders. During the ball milling process, metallic particles are subjected to severe shear stress and therefore their fracture occurs. This ensures the good distribution

of graphene in metal matrix. Also, interfacial attachment between graphene and metal matrix is controlled by various processes occurring during ball milling such as cold welding, particle fracture and rewilding of metallic powders (Chu and Jia, 2014). Dispersion of graphene in metal matrix depends upon various factors such as milling medium, time, atmosphere, graphene content and ball to powder ratio. It is obvious that longer milling time will ensure better dispersion. However, if milling time is too long, this would adversely affect the morphology of graphene (Pérez-Bustamante et al., 2014; Yue et al., 2017). Post blending process includes compaction and consolidation of composite powders. Compaction and consolidation can be carried out in single step such as press sintering (Pérez-Bustamante et al., 2014). Nonetheless, compaction and sintering could be performed in separated stages as well. Furthermore, efficient alternatives have also been employed for consolidation of composite powders (Borkar et al., 2015). For example, spark plasma sintering (SPS) and microwave sintering processes are considered best alternatives of conventional sintering. As the essential outcome of sintering process, however, there is always porosity in the structure which causes in the weakening of properties of the composites. Some researchers have also utilized some further processing on the sintered samples in order to improve properties. These processing techniques include hot extrusion, rolling, annealing etc. (Shin et al., 2015). Extrusion and rolling can help in bringing partial alignment of graphene sheets. Several metals and alloys such as Cu, Ni, Ti based alloys etc. have been processed through MA to incorporate graphene.

1.4.2 Semi Powder Metallurgy (SPM)

SPM, also known as solution mixing, is widely used technique to address the challenges of dispersion and interaction of graphene with metal matrix. SPM is different from MA in a sense that it uses solvent (liquid) to disperse the graphene in metallic powders (Bhaduria, Singh, and Laha, 2019; Chen, Zhang, and Chen, 2012). The advantage of using solution mixing is that it not only provides good mixing but the structure of

graphene is also preserved (Chen, Zhang, and Chen, 2012; Wang et al., 2017).

The process is carried out in the following steps. Initially, graphene reinforcement is dispersed in the solvent by using sonication. This is followed by the mixing with metallic powders (Li et al., 2009). In order to get uniform distribution of graphene, several blending processes such as ball milling, mechanical mixing and ultrasonication are performed on composite powder (Li et al., 2009). Then solvent is removed by filtering process followed by the drying and heat treatment processes under reducing environment to remove any oxides. Next, consolidation is performed either by conventional sintering, hot pressing or SPS (Li et al., 2009). In SPM process, surfactants are also utilized provide better interfacial attachment between graphene and metal particles (Li et al., 2009). These surfactants enhance interaction either by electrostatic interaction or by covalent bonding. This method has tunable processing parameters and can be employed on industrial scale, various materials such as Al, Ni, Cu, Fe, Ti, Mg etc. have been processed by using this technique (Naseer et al., 2019).

1.4.3 Molecular-level Mixing (MLM)

MA and SPM are good at overcoming the graphene dispersion problem. However, due to low wettability of graphene, interfacial bonding between graphene and metal matrices is not strong enough to deliver the desired properties (Li et al., 2009; Clyne and Withers, 1995). Strengthening efficiency can be improved by employing a molecular-level bonding at the interface (Hidalgo-Manrique et al., 2017). In molecular-level mixing technique, graphene sheets are first exfoliated by ultrasonication, then mixed and dispersed with metal salts and lastly, metallic ions are reduced on graphene sheets to give metal-decorated reduced graphene sheets in the form of powder (Young et al., 2018). The most commonly used graphene reinforcement material for MLM is graphene oxide (GO). Presence of functional group on GO surface results in strong interaction between GO and other atoms (Suk et al., 2010; Ruiz-Vargas et al., 2011). Metallic ions find nucleation

sites on GO surface because of the existence of oxygen-based functional groups surface of GO. In this way, strong covalent bonding between metal and carbon atoms due to these functional sites is formed which would not be possible otherwise (Nicholl et al., 2015). The consolidation of the composite powder (metal-decorated reduced graphene) can be carried by conventional sintering processes, hot pressing or SPS (Ahmad, Hashim, and Ghazali, 2007; Oliver and Pharr, 1992).

MLM improves not only wettability between graphene and metal particles but also helps prevent the agglomeration of graphene sheets. Metallic particles attached on the graphene surface during MLM process also act as spacers thereby preventing agglomeration. However, MLM is mostly limited to Cu only because of the ease of the attachment of copper ions on GO surface. Some reports have also included attachment of Ni, Ag, and Mg particles on graphene surface, whilst using metal decorated graphene sheets as reinforcement in Cu, Al, and Ag matrix composites (Xia et al., 2017).

1.4.4 In-situ Growth

In this process, metallic powder is mixed with carbon or hBN source and is subjected to high temperature in a chemical vapor deposition (CVD) furnace. At high temperature, the source dissociates to constituent atoms which diffuse into metal particles at high temperature (Cao et al., 2019). After diffusion, these atoms join together to form graphene (or hBN) surrounding the metal grains. In this way, graphene is dispersed and attached with metal interface without any damage to graphene lattice. Graphene embedded powder can then be consolidated using hot pressing, compaction, and conventional or SPS (Fu et al., 2018). The basics of in situ growth of graphene is simply to grow graphene on metallic particles, which are then subjected to consolidation without the need of any further processing (Chen et al., 2016). Schematic diagram is shown in Figure 1.1. A solid or gaseous carbon source supplies carbon atoms, which undergo deposition at high temperature, typically in a CVD furnace. Similar to other techniques,

many different routes have been investigated for in-situ growth of graphene in metal matrix. Type of carbon source, carbon quantity, growth temperature and growth time are the key parameters which effect the crystallinity, number of layers and hence quality of graphene layers (Liu et al., 2017). In order to enhance distribution of graphene layers, preprocessing is also carefully carried out to ensure a good mixing and hence maximized interaction of carbon source with metallic particles (Guo et al., 2020).

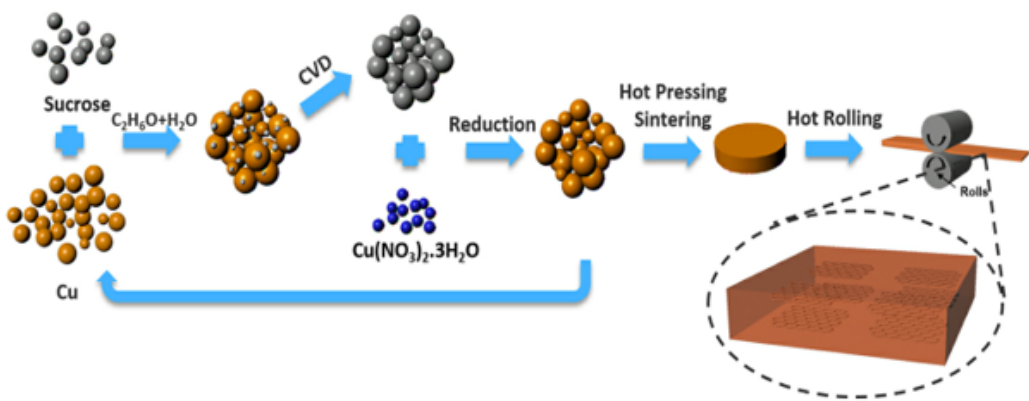


Figure 1.1: Schematic illustration of the in-situ growth for graphene reinforced Cu composite (Guo et al., 2020).

The in-situ processing technique is widely being used because of its simplicity and applicability. The fabrication of composites containing well-ordered (aligned) and uniformly dispersed graphene composites via in-situ method could be economically preferred option (Kawk, Ring, and Choi, 2019). Various studies suggest that strength of materials can be increased without any compromise on their other properties such as thermal and electrical conductivities, corrosion resistance etc. Some researchers (Chen et al., 2016; Liu et al., 2017; Guo et al., 2020) introduced a simple two-step process which comprises simply two steps, i.e. powder compaction and CVD. The spaces in the compacted sample act as catalyst sites (template) for graphene growth during CVD. This method ensures not only uniform dispersion of graphene in matrix but also helps in the formation of three dimensionally interconnected network of graphene surrounding the

grains of matrix (Kawk, Ring, and Choi, 2019). In this way, this process has potential to improve mechanical, thermal, chemical and wear properties simultaneously.

Zhang et al. (Zhang et al., 2020) developed a powder-metallurgy based strategy for fabricating 3DiGr-Cu composites for high-performance advanced structural materials, which involves the rapid thermal annealing (RTA) in situ growth of three dimensionally interconnected network of graphene (3DiGr) on Cu powder. During CVD process, 3DiGr grown on the Cu powders is directly welded and thus construct a 3D interconnected graphene network in the composites due to the coefficient of thermal expansion (CTE)-mismatch related thermal stress between 3DiGr and Cu. In the constructed composites, the highly interconnected feature of 3DiGr could not only endow it with a much larger interfacial shear stress than 2D isolated graphene in the composites for achieving a much better load transfer strengthening capability and a remarkably higher strengthening efficiency, but also greatly reduce the electrons scattering in the interfacial areas and construct extensive conducting highways throughout the matrix for electrons transportation. As a result, the 3DiGr-Cu composite demonstrates superior mechanical properties, electrical and thermal conductivity simultaneously, which has the potential to satisfy many special applications such as lightweight macroscopic conductors and heat-sinks in electronics. Moreover, this feasible and scalable bottom-up concept to welding graphene into a continuous network architecture during powder consolidation can enable new paths to design 3D network structure constructed by 2D building blocks in the metal matrix composites without the ubiquitous restrictions of currently-used melting-related processing methods.

In our research, we proposed an in-situ growth route, which starts from CuNi powders by using a simple two-steps method. Thereby, the overall fabrication process of 3DiGr-CuNi or 3Di hBN-CuNi composites could be primarily divided into two steps. We followed this method for the synthesis of graphene or hBN reinforced CuNi composites and found outstanding results with regards to application and properties.

1.5 Applications of Gr/hBN in MMCs

1.5.1 Mechanical Properties

MMCs reinforced by 2D materials have shown excellent mechanical properties including yield strength, tensile strength, toughness etc. Chu et al. (Chu and Jia, 2014) found that Gr-Cu composite showed enhancement in yield strength and Young's modulus upto 114% and 37%, respectively compared to unreinforced Cu. Chen et al. (Chen et al., 2016) investigated on in-situ grown graphene reinforced Cu matrix composites and found 177% and 27.4% enhancement in yield and tensile strength over pure copper. Similarly, various researchers have observed a substantial increment in mechanical properties of the metal matrix as shown in Table 1.1. Shu et al. (Shu et al., 2019) reported the improved mechanical properties of Cu/Ti₃SiC₂/C nanocomposites due to synergetic effect of graphene and hBN. There are several mechanisms which can explain the reinforcing effect of graphene (or hBN) which are given below:

Table 1.1: Mechanical properties of graphene reinforced MMCs.

| Processing method | Ultimate tensile strength (MPa) (Compared to Cu) | Reference |
|--|---|-------------------------|
| MLM + SPS | 319 (increase 25%) | Li et al., 2015b |
| Sonication + Spark plasma sintering | 131 (decrease 24%) | Li et al., 2014b |
| Ball milling + Equal speed rolling | 315.1 (decrease 0.7%) | Kim, Lee, and Han, 2014 |
| A in-situ two-step process | 218 (increase 20%) | Jo et al., 2019 |
| Sonication + Hot pressing | 271 (increase 18%) | Tang et al., 2014 |
| Ball milling + Sparking plasma sintering | 355 | Cui et al., 2014 |
| In-situ growth + Hot pressing + Hot rolling | 275 (increase 27%) | Guo et al., 2020 |
| Ball milling + In situ growth + Hot pressing | 274 (increase 27.4%) | Chen et al., 2016 |

1.5.1.1 Load Transfer

3DiGr or 3Di-hBN, having strong interfacial bonding to metal matrix can transfer the externally applied load. This network sustains the applied load as a whole instead of as isolated pieces of graphene or hBN layers. Therefore, overall strength of the reinforced composite is enhanced (Chen et al., 2016). Figure explains the role of 3DiGr in increasing

the strength by mechanism of load transfer. When the composite is under stress, graphene sustains a certain part of load transferred from the matrix in the process of deformation. Since graphene has much higher strength than the matrix, the matrix fractures before than graphene. After the fracture of metal matrix, graphene is lengthened and an extra force is needed to achieve the complete fracture of graphene, which can be corroborated by the morphology of the fracture surface. The schematic diagram Figure 1.2 is also helpful to explain the improvement in elongation of graphene/Cu composite.

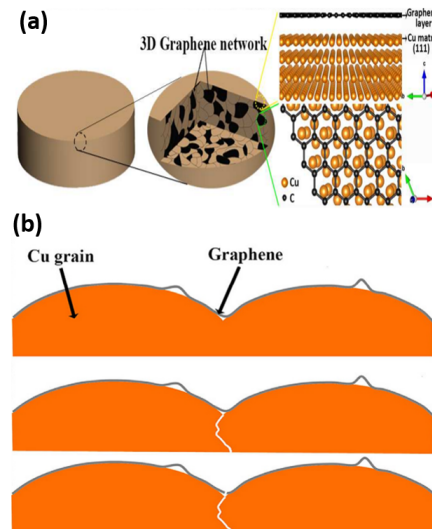


Figure 1.2: Schematic diagrams (a) 3DiGr (black areas) in Gr-Cu composite transferring the load in matrix(Chu et al., 2018b) (b)Section view of graphene/Cu in the fracture process, the graphene delays the fracture under the mechanism of load transfer (Chen et al., 2016).

1.5.1.2 Dislocation Strengthening

When external load is applied on the composite, the graphene or hBN can act as a barrier to inhibit the dislocation motion, leading to the dislocation accumulation nearby the interface (Kim et al., 2013). Chu et al. (Chu et al., 2018b) explained that improved tensile properties of Gr-Cu composites can be attributed to the accumulation of dislocations at metal-graphene interfaces after tensile deformation, identified by transmission electron

microscope (TEM) and X-ray diffraction (XRD) analyses.

1.5.1.3 Grain refinement

The inclusion of graphene or hBN in the metal matrix is quite likely to inhibit the grain growth during the synthesis process which leads to refinement in the structure (Chu and Jia, 2014). The grain size affects the yield and tensile strength of the sample according to the classic Hall-Petch equations (Kato, 2014; Zhang et al., 2017b):

$$\sigma_{YS} = \sigma_{YS} + k_{YS}d^{-1/2} \quad (1.1)$$

$$\sigma_{UTS} = \sigma_{UTS} + k_{UTS}d^{-1/2} \quad (1.2)$$

where, σ_{YS} and σ_{UTS} correspond to the yield strength and the ultimate tensile strength, respectively. These equations indicate that the strength of a material increases with the decrease in grain size.

1.5.2 Thermal properties

Graphene has high thermal conductivity, so its inclusion in the metal matrix composite would increase the thermal conductivity. Zhang et al. (Zhang et al., 2020) found that three-dimensional network of graphene in Cu matrix contributed to more than 10% increment in thermal conductivities. They explained their findings by conducting molecular dynamic simulations to prove that three-dimensional network of graphene provides effective conducting path channel for electrons and phonons motion. Li et al. (Li, Ring, and Choi, 2019) adopted a simple two-step process route to fabricate three dimensionally interconnected network of graphene Cu composite and found a substantial increase in thermal conductivity. Table summarizes the thermal conductivity of graphene reinforced Cu composites produced via various processing methods.

Table 1.2: Thermal conductivities of graphene reinforced MMCs.

| Processing methods | Thermal conductivity | Reference |
|--|--|-------------------------------|
| Electrodeposition | 300.5 (increase 5%) | huang2016preparation |
| MLM + SPS | P 362 (decrease 3%) P 345 (decrease 8%) | chen2016effects |
| Stirring + Hot pressing | 370 (increase 3%) | gao2016mechanical |
| Pasting on Cu foil | 445.91 (increase 34%) | hsieh2017synthesis |
| Direct deposition of graphene on Cu foil Stacking +SPS | 359 (increase 8%) | wejrzanowski2016thermal |
| Ball milling+ SPS | P 409 (increase 225%) P 385 (increase 208%) | li2019thermal |
| In-situ two-step process | 296 (increase 15%) 294 (decrease 18%) | luo2017copper si2017effect |
| Ball milling Hot pressing | P 253 P 170 | ponraj2017effect |
| MLM SPS | P 375 (increase 10%) | chu2018thermal |
| Ball milling Hot pressing | P 150 (decrease 10%) | |
| Sonication and vortex mixing Vacuum infiltration SPS | | |

1.5.3 Corrosion Properties

One of the important applications of 2D materials is their ability to increase the corrosion resistance of MMCs. Graphene and hBN are impermeable to ions, molecules and atoms (Mahvash et al., 2017). Therefore, they can hamper the transfer of ions and molecules across the interface and increase the corrosion resistance of the composite. Mahveash et al. (Mahvash et al., 2017) reported that the CVD grown hBN reduces the Cu corrosion rate by an order of magnitude compared to bare Cu. Li et al. investigated the corrosion resistance of three-dimensionally interconnected networked graphene-Cu composite by potentiodynamic polarization tests and concluded that three-dimensional graphene structure effectively protected the Cu against corrosion. Because of impermeability, graphene or hBN does not let atomic hydrogen entering in the atomic structure and therefore can significantly enhance the resistance of metals and alloys to hydrogen embrittlement. Nam et al. (nam2014graphene) reported that graphene coating could be a protective barrier against the hydrogen embrittlement. Li et al., through the series of electrochemical experiment, also reported the higher tendency of three dimensionally interconnected graphene reinforced Cu composite to block the penetration of atomic hydrogen.

1.6 Summary

In summary, graphene and hBN has a large potential to reinforce the chemical, mechanical and thermal properties of metal matrix composites due to their outstanding properties. We found that there are several studies which discuss the properties of metal matrix composites reinforced by 3DiGr. However, a very limited amount of research has been done on the metal matrix composites reinforced by 3Di-hBN, despite the fact hBN has also has excellent mechanical, thermal and chemical properties. Therefore, in this dissertation, we particularly explored the applications of hBN in the CuNi matrix. We reported the mechanical, corrosive, high temperature oxidation, and thermal properties of 3Di-hBN reinforced CuNi composites fabricated by using a simple two-step process. Nevertheless, we also fabricated 3DiGr reinforced CuNi composite, and determined their scope to be used in the energy field.

2 Synthesis of Three-Dimensionally Interconnected Hexagonal Boron Nitride Networked Cu-Ni Composite

2.1 Introduction

The development of two-dimensional (2D) materials has opened up the possibilities for their application in improving the properties of metals and alloys (Bartolucci et al., 2011; Chu and Jia, 2014; Yang et al., 2018; Li, Ring, and Choi, 2019). This is because 2D materials have the potential to alter the properties of metals at the nanoscale. A single layer of hexagonal boron nitride (hBN) is structurally similar to graphene (carbon system) where the hexagonal lattices are occupied by boron and nitrogen atoms. hBN has a lattice parameter of 25 nm and possesses extraordinary properties, such as high chemical stability (Singh, Joshi, and Singla, 2018), high mechanical strength (Singh, Joshi, and Singla, 2018), low density (Elkady et al., 2015), high thermal stability (Liu et al., 2013), and high thermal shock resistance (Duan et al., 2016). These excellent properties can be utilized to improve the performance of various metal matrix composites (MMCs) through the in-situ construction of three-dimensionally interconnected (3Di) hBN layers in their grain boundaries. Similar approaches have been employed by other researchers, who used 3D- networked graphene to tailor the properties of MMCs (Li, Ring, and Choi, 2019; Chen et al., 2016; Kim and Shon, 2018; Song, Kwak, and Choi, 2018). For instance, Chen et al. (Chen et al., 2016) enhanced the yield and tensile strengths of copper by wrapping graphene around copper grains using chemical vapor deposition (CVD). They reported that the graphene acted as a barrier for dislocation movement, and consequently, the elastic modulus and strength were improved. Xue et al. (Li, Ring, and Choi, 2019) reported that Cu-graphene composites had a higher thermal conductivity than pure copper because graphene offered an effective path for heat transfer between the Cu grain boundaries. Other properties, such as corrosion resistance and wear resistance, have also been improved (Wu et al., 2019; Tripathi, Gyawali, and Lee, 2017).

Because of its structure similarity with graphene, the hBN introduced to metal matrices can also impart similar effects. Several researchers have used boron nitride nanoparticles to enhance the strength, hardness, wear, and corrosion resistance of metallic alloys (Gopinath, Prince, and Raghav, 2020; Reddy, 2013; Zitoun and Reddy, 2008; Khatavkar et al., 2018; Cho and Shon, 2018). For instance, the microstructure and properties of BN/Ni-Cu composites fabricated by powder technology were reported by Tantaway et al. (El-Tantawy, Daoush, and El-Nikhaily, 2018). They found that the BN content led to a decrease in density and an increase in the hardness, electrical resistivity, and saturation magnetization of the composite. Omayma et al. (Elkady et al., 2015) fabricated Cu/hBN nanocomposites by the PM route, in which powder mixtures of Cu and hBN were compacted and sintered at various temperatures ranging from 950°C to 1000°C. They found that the physical, mechanical and tribological properties of the composite were influenced by the hBN. However, we have not found any published studies in which metal matrices were reinforced by a 3Di network of hBN layers.

Recently, various techniques have been utilized to fabricate reinforced MMCs through the incorporation of graphene. For instance, Xiong et al. (Li et al., 2015a) introduced graphene in Cu by the reduction of reduced graphene oxide through sintering. Similarly, ball milling, molecular-level synthesis, spark plasma sintering, and epitaxial growth have been used to improve the strength of composites using graphene as a reinforcement (Chen et al., 2016; Cao et al., 2017; Jiang et al., 2016; Wang et al., 2019). However, each of the these strengthening techniques has some limitations. For instance, ball milling and molecular-level mixing may allow a uniform dispersion of the reinforcement material but may impart structural defects due to the shear stress and the contamination during the fabrication process (Naseer et al., 2019). A well-ordered/-aligned, uniformly dispersed, and continuous graphene network is essential to attain the best reinforcement results (Chen et al., 2016). Kawk et al. (Kawk, Ring, and Choi, 2019) introduced a simple, economically efficient two-step process with the potential to deliver

better-quality products with uniformly dispersed and continuous graphene networks.

The two-step process involves the compaction of a metallic powder followed by CVD. In this study, we fabricated a 3Di-hBN-Cu-Ni composite using a similar simple two-step process. Various characterization techniques were employed to confirm the formation of 3Di-hBN surrounding the grains of the Cu-Ni alloys. Cu-Ni-based alloys have been applied in various industries, such as shipbuilding, construction, and processing, owing to their high mechanical strength and corrosion resistance at elevated temperatures. The 3Di-hBN-Cu-Ni composite is expected to deliver better corrosion, mechanical, and wear characteristics than the Cu-Ni alloy. Moreover, the 3Di-hBN layer, a foam-like 3D porous structure, was separated from the 3Di-hBN-Cu-Ni composite. Such a 3Di-hBN material can be applied in the fields of biomedicine, electronics, and energy storage (Gautam et al., 2018; Guiney et al., 2018; Yin et al., 2013).

2.2 Fabrication of 3Di-hBN CuNi Composite

2.2.1 Compaction of CuNi powders

A simple two-step process involves the compaction of powder particles in a mold followed by CVD. Cu powder (99.5 % purity) with spheroidal particles of size 14–25 μm and Ni powder (>99.5% purity) with spheroidal particles of size 1 μm were purchased from Sigma-Aldrich and used after heat treatment (200°C for 2 h in an H₂ environment) to remove any moisture or oxide contents. The chemical compositions of Cu and Ni powders are provided in Table 2.1. Cu and Ni powders (70 wt.% Cu, 30 wt.% Ni) were mixed manually using mortar with care not to change the particle size distribution and the mixture was compacted in a mold using a double-action oil hydraulic press at the compaction pressures of 60, 110, 220, 280, 335, and 390 MPa as shown schematically in Figure 2.1. The exertion of high pressure on the spheroidal particles caused mechanical cold locking among the particles, thus forming a compact disc with the approximate diameter and thickness of 15 mm and 1.2 mm, respectively. As shown on the fracture

surface of the cross section of the compact disc in Figure 2.2, relatively large Cu particles produced mechanical interlocking owing to their deformation, and Ni particles filled the gaps between the Cu particles.

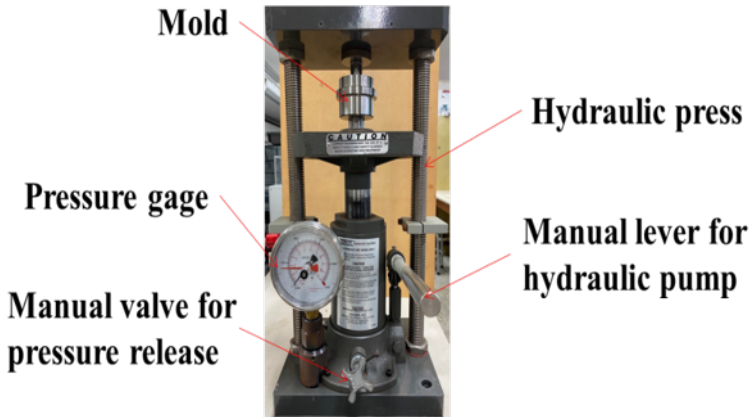


Figure 2.1: Mold and hydraulic press used for powder compaction.

Table 2.1: Chemical compositions of Cu and Ni powders.

| Material | Purity | Trace metals in ppm |
|----------|--------|---|
| Cu | >99.5% | Fe 80.0, Na 9.42, Mn 7.6, Mg 4.69, Al 4.4, and B 1.98 |
| Ni | >99.5% | Ag 1.3, Al17.9, Ba 0.8 Ca 27.9, Cr 3.6, Cu 305.2, Fe 383.7 Mg 2.0, Mn 2.6, Na 11.1, Pd 8.0, Ti 144.5, and V 25.4 |

2.2.2 Metal Organic Chemical Vapor Deposition

The discs were then placed in a quartz glass tube furnace with a tube diameter of 23 mm for metal-organic CVD (MOCVD). The compaction pressure and sintering time were varied to determine the optimum conditions for the fabrication of 3Di-hBN in 3Di-hBN-Cu-Ni composite. Figure 2.3 (a) shows a schematic of the system used to fabricate the 3Di-hBN-Cu-Ni composites. Initially, the system was flushed with argon at least three times to remove air from the MOCVD tube. The furnace temperature was increased to 400°C at a rate of 16.6°C/min and then maintained constant in a hydrogen environment at

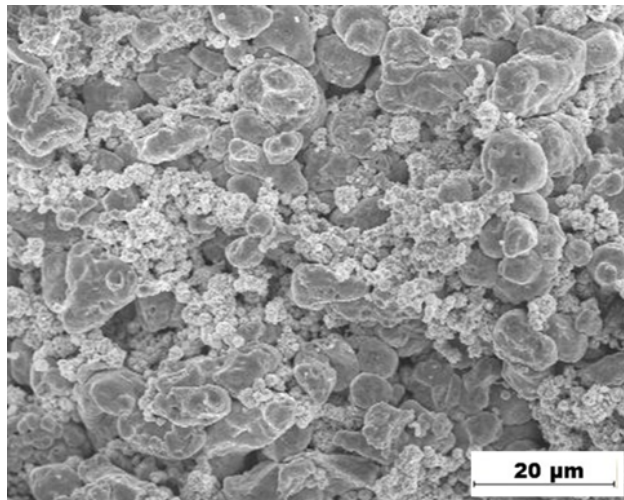


Figure 2.2: Cu and Ni particles shown at the fracture surface of the disc after compaction.

330 Torr for 1 h for deoxidation. Subsequently, the temperature was raised to 1000°C at the same rate and maintained constant for 15 or 30 min. Finally, MOCVD was performed for 15 min at 450 Torr using heated decaborane ($B_{10}H_{14}$) as the boron source and ammonia (NH_3) as the nitrogen source. Decaborane was the preferred boron precursor because of its (i) easy handling, (ii) commercial availability, and (iii) stability, which minimized the formation of undesired side products at elevated temperatures that could potentially decrease hBN yield (Chatterjee et al., 2012). Decaborane is a crystalline solid with a melting temperature of 98–100°C and its vapor pressure can be easily controlled by varying the temperature from room temperature to 100°C. At approximately 100°C, the vapors produced upon evaporation can be transported into the MOCVD growth zone by an inert carrier gas (Ar) at a flow rate of 1 sccm. Ammonia gas was introduced as a nitrogen source in the MOCVD reaction zone at a flow rate of 2 sccm. At 1000°C, ammonia and decaborane dissociated into nitrogen and boron atoms, respectively.



The entire process (heating, sintering, and MOCVD) was conducted at a hydrogen flow rate of 10 sccm. The 3Di-hBN-Cu-Ni composite fabricated using a simple two-step process is shown in Figure 2.3 (b).

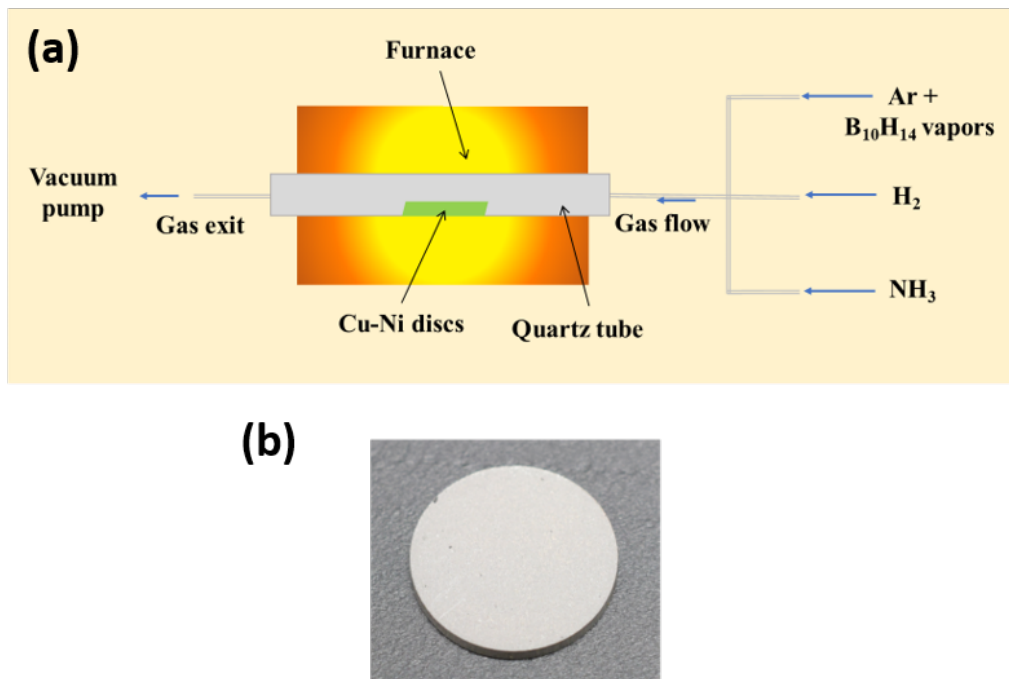


Figure 2.3: (a) Schematic illustration of the fabrication of 3Di-hBN-Cu-Ni composite and (b) disc-shaped 3Di-hBN-Cu-Ni composite fabricated using a simple two-step process.

2.3 Characterization of 3Di hBN-CuNi Composites

2.3.1 Green and Composite Density

Density measurements were made for at least three important reasons: (1) for the determination of mass and volume of samples, (2) the quality of the samples and (3) selecting the optimal experimental condition. Sample density varies with powder size, compaction pressure and experimental condition of CVD. Green density is determined by taking the ratio of compacted CuNi disc to its volume. The densities of synthesized 3Di hBN-CuNi composites were measured using Archimedes principle. The entire procedure is mentioned in Appendix “A”.

2.3.2 Microstructural Characterization

Optical microscopy (OM) and scanning electron microscopy (SEM) investigations of the 3Di-hBN-Cu-Ni composite samples were conducted after the sample was cut in half and the cutting surface was polished with emery papers of size down to 4000 grit. Finally, the polished surface was etched at room temperature using a mixed solution of 1 M FeCl_3 and 0.1 M HCl to reveal the microstructure (Kawk, Ring, and Choi, 2019). The procedure to make this etchant is given in Appendix “B”. For transmission electron microscopy (TEM) investigations, the 3Di-hBN-Cu-Ni composite samples were mechanically polished to a thickness of 100 μm and cut into small pieces of 3 mm diameter. Then, Cu-Ni was etched out, leaving only 3Di-hBN foam, which was transferred after thorough cleaning to the TEM grid for investigation. A qualitative phase analysis of the 3Di-hBN-Cu-Ni composite was performed by XRD analysis using Cu K α radiation with a wavelength of 1.54 \AA and a scanning angle of 20°–100°. To obtain 3Di-hBN foam, the 3Di-hBN-Cu-Ni composite samples were cut into small pieces, polished, and placed in an etchant for a sufficient duration to etch out Cu-Ni completely such that only 3Di-hBN remained. Then, the foam-like 3Di-hBN samples were removed and washed several times with deionized

water. To obtain a stable 3D structure of 3Di-hBN, the freeze-drying method was used to ensure that there was no effect of liquid capillary force and that 3Di-hBN did not structurally collapse (Ding et al., 2017).

2.3.3 Mechanism of hBN Formation at Grain Boundaries

Figure 2.4 shows a schematic of the processes involved in the synthesis of the 3Di-hBN-Cu-Ni composite. During the sintering, the reduction in volume and the formation of Cu-Ni solid solution occur due to the diffusion of metals under the driving force to reduce the excess surface energy (German, 2010; McDonald et al., 2017). Consequently, the overall volume of the compact disc is reduced and densification occurs. The formation of 3Di-hBN in the composite is likely to occur in three stages (Li, Ring, and Choi, 2019). First, the diffusion of metal occurs to reduce the surface energy resulting in the formation of large particles (consolidation). At the same time, the diffusion of Ni to Cu or vice versa occurs to form a solid solution of Cu-Ni. Next, during the MOCVD process, the dissociation of ammonia and decaborane produces nitrogen and boron atoms that diffuse into the Cu-Ni alloy at 1000°C. Finally, upon cooling, the nitrogen and boron atoms precipitate out and alternately join together to form 2D hBN layer(s) along the interfaces of the Cu-Ni grains (Joshi et al., 2012) resulting in the formation of Cu-Ni composite.

Small pores or voids can form during the sintering as Cu and Ni particles grow to reduce their surface energy. This is probably due to insufficient sintering time or excessive free space among the particles. These pores may also act as catalytic sites for the nucleation and growth of bulk hBN. The small lighter grey areas (indicated by small white loops) in Figure 2.5 indicate the bulk hBN that accumulated on the pores during the MOCVD process. These pores generated during the sintering process and then filled with bulk hBN during the MOCVD process are undesirable, as they may adversely affect the mechanical, thermal, and wear characteristics of the composite. Therefore, the processing parameters, such as compaction pressure and sintering time, must be varied

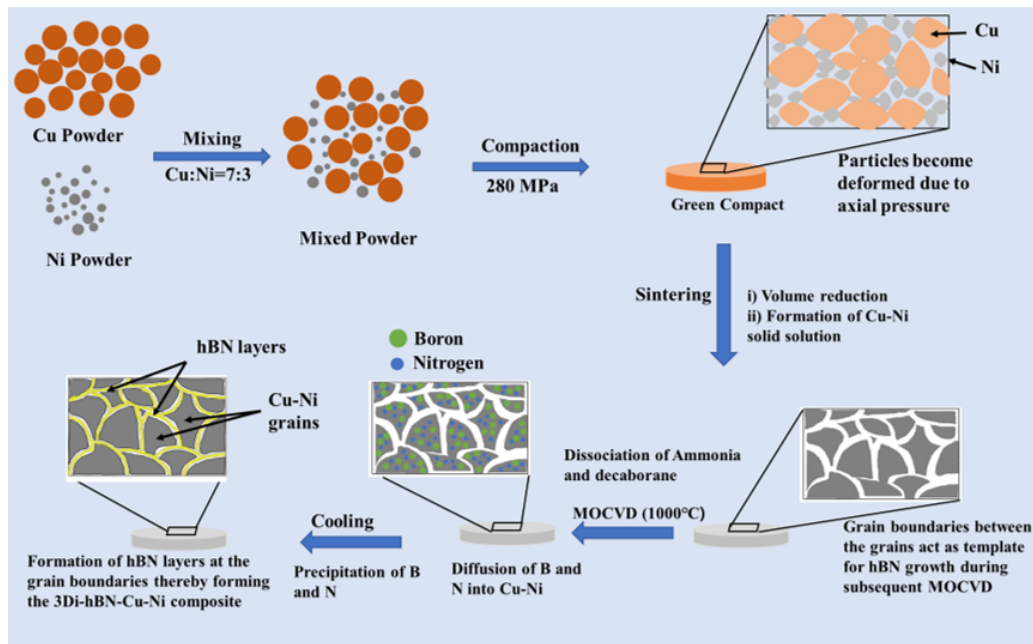


Figure 2.4: Schematic showing the process of formation of 3Di-hBN-Cu-Ni composite.

to determine the optimal conditions for the fabrication of 3Di-hBN-Cu-Ni composites without the formation of bulk hBN.

2.4 Optimal Conditions of Constructing 3Di-hBN in 3Di hBN-CuNi composite

Figure 2.6 shows the density of the 3Di-hBN-Cu-Ni composite as a function of the compaction pressure and sintering time. The density of the composite increased with increasing compaction pressure. However, beyond a certain compaction pressure, the density decreased. This trend occurred because at pressures below 280 MPa, the compaction pressure was not enough resulting in low density of compaction; consequently, resulting in lower density of composite having voids or pores. Although these pores were filled with bulk hBN during the subsequent MOCVD process, the overall density of the composite cannot be increased because the density of hBN (2.1

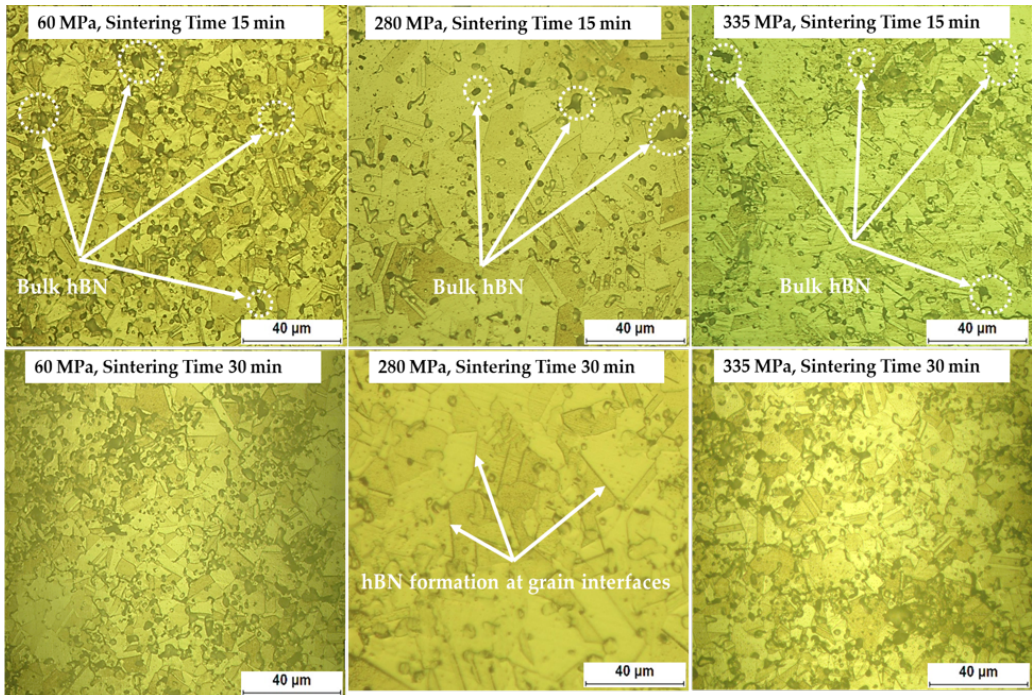


Figure 2.5: OM images of 3Di-hBN-Cu-Ni composites under various conditions.

g.cm^{-3}) is significantly lower than that of Cu-Ni (8.9 g.cm^{-3}). On the other hand, during compaction at high pressures (280 MPa), the particles on the surface were pressed with a relatively greater force than those inside the compact disc because of the friction between the particles. Consequently, at pressures exceeding 280 MPa, the surface particles of the compact disc were denser than the inner particles. The inner particles having a longer diffusion distance owing to their lower density resulted in the formation of pores due to insufficient diffusion or a short sintering time, resulting in relatively larger size of pores or shrinkage as indicated by OM images in Figure 2.7(b). Hence, the density of the 3Di-hBN-Cu-Ni composite was slightly lower at higher pressures ($> 280 \text{ MPa}$) as shown in Figure 2.6. This is also evident from the OM images shown in Figure 2.5. The white arrows in Figure 2.5 indicate the bulk hBN present in the microstructure of the 3Di-hBN-Cu-Ni composite. Relatively higher volume fraction of bulk hBN was observed when the

compaction pressure is lower or higher than 280 MPa. Furthermore, the density of the 3Di-hBN-Cu-Ni composite also depends on the sintering time as shown in Figure 2.6. A longer sintering time led to fewer pores (i.e. lower volume fraction of bulk hBN), and consequently more densification occurred.

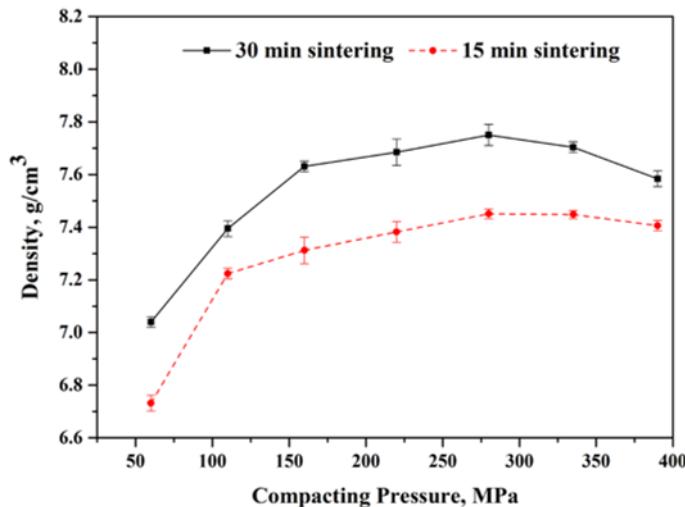


Figure 2.6: Density of the 3Di-hBN-Cu-Ni composite as a function of compacting pressure and sintering time.

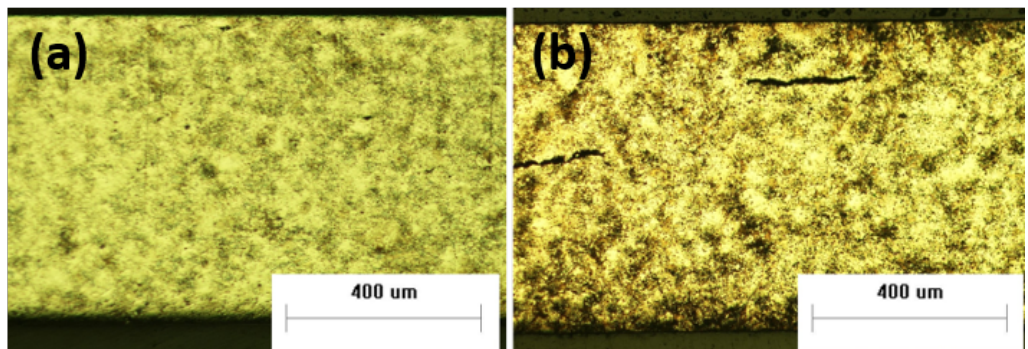


Figure 2.7: OM images of 3Di hBN-Cu-Ni composites processed at compaction pressures of (a) 280 MPa and (b) 335 MPa.

2.5 Microstructural Investigation

The 3Di-hBN-Cu-Ni-hBN composite, fabricated under the optimized conditions (compaction pressure of 280 MPa and sintering time of 30 min) was examined using SEM. While some of the bulk hBN was removed during the polishing and etching, the SEM image in Figure 7 and the EDS results in Table 2 show the Cu-Ni grains, bulk hBN of less than 5 μm in size, and hBN along the interfaces. The Cu-Ni grains, grain boundaries, and bulk hBN in Figure 2.8 were analyzed using energy-dispersive X-ray spectroscopy (EDS). Boron and nitrogen were observed (locations (a) and (b) in Figure 2.8) in excess along with minute amounts of other impurities, such as silicon, carbon, and oxygen, as listed in Table 2.2. These impurities probably entered the structure during polishing and etching processes. Location (a) in Figure 2.8 is a pore that was first formed as a consequence of sintering and then filled with bulk hBN during the subsequent MOCVD process. Considering the average size (5 μm) of these sites (location (a)), the presence of bulk hBN was verified through EDS analysis. Further EDS analysis at the grain boundaries (location (b)) revealed that the grain boundaries were also mostly occupied by boron and nitrogen with approximate stoichiometric ratio of 1:1. As expected, the Cu-Ni grains (location (c) in 2.8) comprised Cu and Ni atoms with a ratio of approximately 7 to 3, as shown in Table 2. The solubility of B and N in Cu-Ni alloy at 1000°C is very small (ppm) (El-Tantawy, Daoush, and El-Nikhaily, 2018) and most of the atoms (B and N) precipitated out during cooling thus forming hBN with B and N having stoichiometric ratio of 1:1 at grain boundaries (Khan et al., 2017; Koepke et al., 2016).

Table 2.2: EDS results of the 3Di-hBN-Cu-Ni composite for the microstructure shown in Figure 2.8.

| Element | Location | Cu | Ni | B | N | Si | C | O |
|---------|-------------------|-------|-------|-------|-------|------|------|------|
| At. % | (a) in Figure 2.8 | - | - | 49.32 | 47.45 | 0.76 | 0.87 | 0.68 |
| At. % | (b) in Figure 2.8 | 20.51 | 8.32 | 34.26 | 34.82 | 0.89 | 0.57 | 0.78 |
| At. % | (c) in Figure 2.8 | 71.28 | 28.42 | - | - | - | - | - |

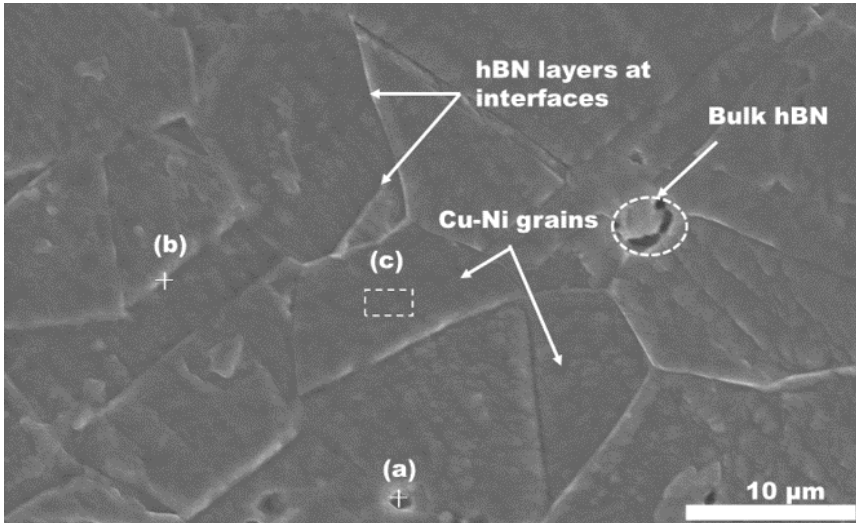


Figure 2.8: SEM image showing the surface morphology of the 3Di-hBN-Cu-Ni composite fabricated with compaction pressure of 280 MPa and sintering time of 30 min.

The SEM image in Figure 2.9 shows various hBN layers that interconnect to form a foam-like structure with pockets and channels. The channels are the connected areas between the Cu-Ni grains formed by etching. The average pocket size ($10\text{-}20 \mu\text{m}$) in 3Di-hBN (Figure 2.9) is approximately equal to the average grain size of the 3Di-hBN-Cu-Ni composite (Figures 2.5 and 2.8) indicating that the hBN layers wrapped around the Cu-Ni grains in the 3Di-hBN-Cu-Ni composite.

The XRD pattern of 3Di-hBN-Cu-Ni composite is shown in Figure 2.10 (a). This pattern shows the crystalline phase of Cu-Ni solid solution only. Moreover, the elemental distribution map of the 3Di-hBN-Cu-Ni composite shown in Figure 2.10 (b) shows uniform distribution of Cu and Ni indicating the formation of Cu-Ni solid solution.

The 3Di-hBN foam was inspected using TEM. The low-magnification bright-field TEM image in Figure 2.11(a) shows a complex morphology with curvatures and overlapped structures where the 3D layers of hBN (shown in Figure 2.9) collapsed after their transfer to the TEM grid under the capillary force acting during the drying process. The selected-area electron diffraction pattern of 3Di-hBN (inset in Figure

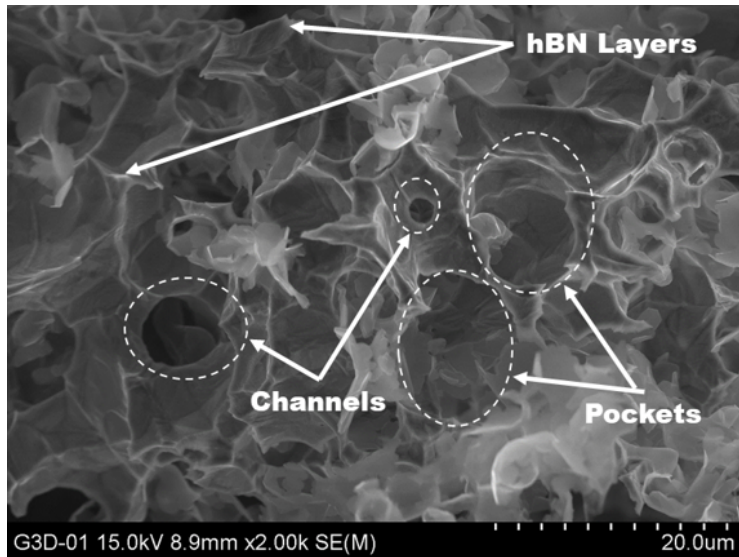


Figure 2.9: SEM image showing the 3D interconnected network of hBN in 3Di hBN-Cu-Ni composite produced under compaction pressure of 280 MPa and sintering time of 30 min, respectively.

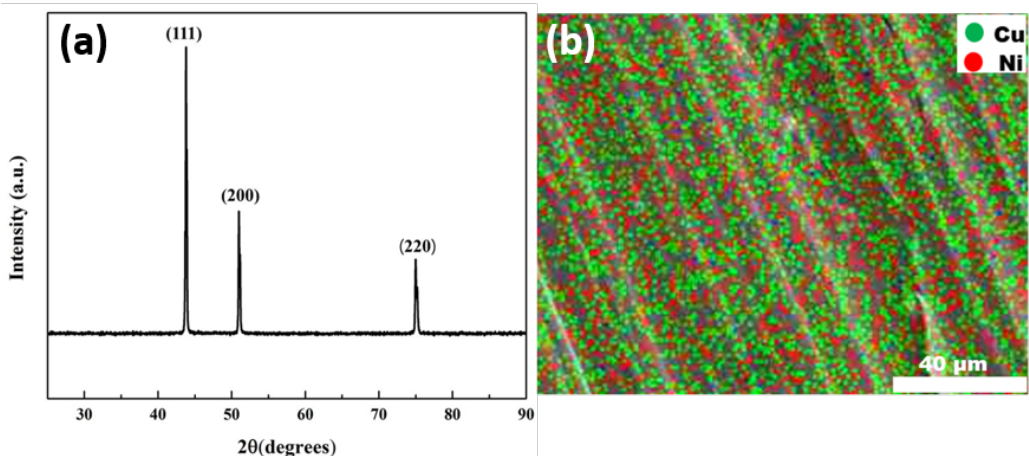


Figure 2.10: (a) XRD pattern of 3Di-hBN-Cu-Ni composite and (b) Elemental distribution map of 3Di-hBN-Cu-Ni composite.

[2.11\(a\)](#)) indicates multiple orientations associated with a couple of layers with different orientations. The high-resolution TEM (HR-TEM) image ([2.11 \(b\)](#)) reveals 2–6 layers of hBN with an interlayer distance of approximately 0.25 nm (inset in Figure 10(b)), which

is attributed to the thickness of a single layer of 2D hBN.

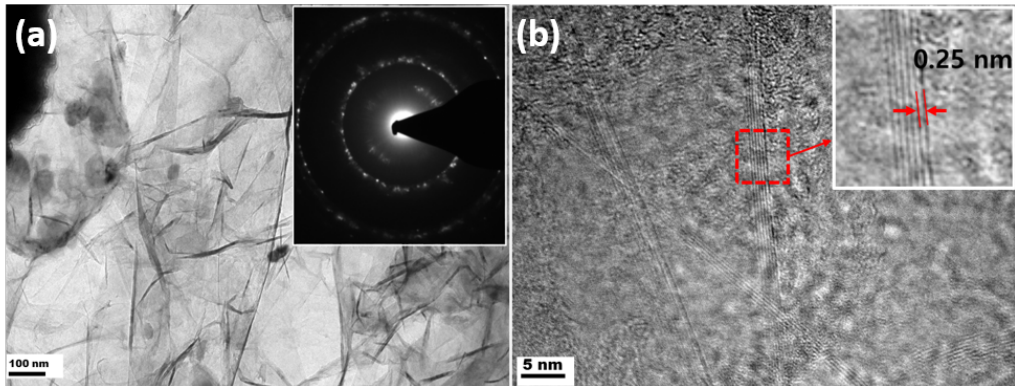


Figure 2.11: TEM investigation: (a) low-magnification bright-field TEM image of 3Di-hBN; (b) HR-TEM image showing 2–6 layers of hBN; inset shows a distance of 0.25 nm between layers.

In summary, 3Di-hBN-Cu-Ni composites were synthesized via a simple two-step process of (1) the compaction of Cu and Ni powder mixtures without any additives and (2) MOCVD. The density of the composite was the highest (7.75 g.cm^{-3}) when the compaction pressure and sintering time were 280 MPa and 30 min, respectively. OM, SEM, and TEM images indicated that these conditions were optimal for the growth of the interconnected network of hBN in the 3Di-hBN-Cu-Ni composite. SEM investigations and EDS analysis revealed that the grain boundaries were mostly occupied by boron and nitrogen atoms. 3Di-hBN was obtained after etching the Cu-Ni and the average pocket size of the foam was 10–20 μm . The 3Di-hBN-Cu-Ni composite with a density of 7.75 g.cm^{-3} was shown to have a three-dimensional network of 2D hBN. The structural investigation of 3Di-hBN through TEM revealed 2–6 layers with an interlayer distance of 0.25 nm. This study can be extended further for the characterization of the physical and chemical properties of 3Di-hBN-Cu-Ni composite and 3Di-hBN.

3 SUMMARY AND CONCLUSIONS

The results presented in this paper certainly place the proposed approach as a competitive methodology for designing fault-resilient circuits. SYFR is a complete systematic method for automated synthesis of fault-resilient circuits at the gate-level without considering technology-specifics. Since SYFR is based on evolutionary computation, it is able to provide a multitude of tradeoffs in comparison to the conventional synthesis tools. The circuits evolved can easily be inserted at intermediate nodes without creating any single points of failure.

The superior performance of fault-resilient circuits at intermediate nodes was demonstrated through an application on artificial neural networks. Results give credibility to the fault-resilience metric P_{fault} used by SYFR to characterize a circuit's tolerance to faults. The majority of SYFR's synthesis success is attributed to the proposed strategy for constraining the Cartesian graph. The graph constraints made the evolution much easier as confirmed by experimental results. It was also demonstrated that smaller fault-resilient arithmetic circuits can be stacked to build large adders and multipliers which are also fault-resilient.

Another benefit of SYFR was that it does not require any special computational resources to execute. A modern desktop-class computer can easily implement SYFR since all of our experiments were conducted on a desktop-class machine.

For future research, we plan to investigate ways to utilize circuits from ReCkt library to build larger arithmetic circuits in an optimal way. We also intend to investigate the evolutionary synthesis of error-resilient circuits. That is to say, there are different error metrics which are application-oriented. For example, PSNR is a metric which is used to gauge the quality of an image. Our goal would be to apply evolutionary circuit synthesis in such a way that the circuits are evolved for improved PSNR performance in fault conditions.

PUBLICATIONS

1. Umar Afzaal, Abdus Sami Hassan, Muhammad Usman and Jeong A. Lee. "On the Evolutionary Synthesis of Fault-resilient Arithmetic Circuits". IEEE Transactions on Evolutionary Computation. (2021) (Under review at the time of thesis submission)
2. Umar Afzaal, Abdus Sami Hassan, and Jeong-A. Lee. "Improved error detection performance of logic implication checking in FPGA circuits." Microprocessors and Microsystems 78 (2020): 103179.
3. Umar Afzaal, and Jeong-A. Lee. "Trading the Reliability of Approximate TMR in FPGAs with the Cost of Mitigation." 2020 23rd Euromicro Conference on Digital System Design (DSD). IEEE, 2020.
4. Abdus Sami Hassan, Umar Afzaal, Tooba Arifeen, and Jeong A. Lee. "Input-Aware Implication Selection Scheme Utilizing ATPG for Efficient Concurrent Error Detection." MDPI Electronics 7, no. 10 (2018): 258.
5. Inayat Ullah, Zahid Ullah, Umar Afzaal, and Jeong-A. Lee. "DURE: An energy-and resource-efficient TCAM architecture for FPGAs with dynamic updates." IEEE Transactions on Very Large Scale Integration (VLSI) Systems 27, no. 6 (2019): 1298-1307.
6. Umar Afzaal, and Jeong-A. Lee. "Low-cost Hardware Redundancy for Fault-mitigation in Power constrained IoT Systems." 2020 International Conference on Information and Communication Technology Convergence (ICTC). IEEE, 2020.

BIBLIOGRAPHY

- Novoselov, Kostya S et al. (2004). “Electric field effect in atomically thin carbon films”. In: *science* 306.5696, pp. 666–669.
- Xu, Mingsheng et al. (2013). “Graphene-like two-dimensional materials”. In: *Chemical reviews* 113.5, pp. 3766–3798.
- Zhang, Kailiang et al. (2017a). “Two dimensional hexagonal boron nitride (2D-hBN): synthesis, properties and applications”. In: *Journal of Materials Chemistry C* 5.46, pp. 11992–12022.
- Jiang, HX and JY Lin (2014). “Hexagonal boron nitride for deep ultraviolet photonic devices”. In: *Semiconductor Science and Technology* 29.8, p. 084003.
- Hui, Fei et al. (2016). “On the use of two dimensional hexagonal boron nitride as dielectric”. In: *Microelectronic Engineering* 163, pp. 119–133.
- Constantinescu, Gabriel C and Nicholas DM Hine (2016). “Multipurpose black-phosphorus/hBN heterostructures”. In: *Nano letters* 16.4, pp. 2586–2594.
- Bao, Jie et al. (2016b). “Two-dimensional hexagonal boron nitride as lateral heat spreader in electrically insulating packaging”. In: *Journal of Physics D: Applied Physics* 49.26, p. 265501.
- Oh, Keun-Hwan et al. (2014). “Enhanced durability of polymer electrolyte membrane fuel cells by functionalized 2D boron nitride nanoflakes”. In: *ACS applied materials & interfaces* 6.10, pp. 7751–7758.
- Chimene, David, Daniel L Alge, and Akhilesh K Gaharwar (2015). “Two-dimensional nanomaterials for biomedical applications: emerging trends and future prospects”. In: *Advanced Materials* 27.45, pp. 7261–7284.
- Li, Lu Hua and Ying Chen (2016). “Atomically thin boron nitride: unique properties and applications”. In: *Advanced Functional Materials* 26.16, pp. 2594–2608.
- Li, Lu Hua et al. (2014a). “Strong oxidation resistance of atomically thin boron nitride nanosheets”. In: *ACS nano* 8.2, pp. 1457–1462.

- Kumar, Rajesh, G Rajasekaran, and Avinash Parashar (2016). “Optimised cut-off function for Tersoff-like potentials for a BN nanosheet: a molecular dynamics study”. In: *Nanotechnology* 27.8, p. 085706.
- Wang, Zifeng et al. (2016). “Fabrication of boron nitride nanosheets by exfoliation”. In: *The Chemical Record* 16.3, pp. 1204–1215.
- Bao, Jie et al. (2016a). “Synthesis and applications of two-dimensional hexagonal boron nitride in electronics manufacturing”. In: *Electronic Materials Letters* 12.1, pp. 1–16.
- Nam, Tae-Heum et al. (2014). “Graphene coating as a protective barrier against hydrogen embrittlement”. In: *International journal of hydrogen energy* 39.22, pp. 11810–11817.
- Lee, Changgu et al. (2008). “Measurement of the elastic properties and intrinsic strength of monolayer graphene”. In: *science* 321.5887, pp. 385–388.
- Calizo, Irene et al. (2009). “Raman nanometrology of graphene: Temperature and substrate effects”. In: *Solid State Communications* 149.27-28, pp. 1132–1135.
- Ahn, Jong-Hyun et al. (2014). “Things you could do with graphene”. In: *Nat Nanotechnol* 9, pp. 737–747.
- Balandin, Alexander A et al. (2008). “Superior thermal conductivity of single-layer graphene”. In: *Nano letters* 8.3, pp. 902–907.
- Neto, Antonio Castro, Francisco Guinea, and Nuno Miguel Peres (2006). “Drawing conclusions from graphene”. In: *Physics world* 19.11, p. 33.
- Littlejohn, Samuel David (2013). *Electrical properties of graphite nanoparticles in silicone: Flexible oscillators and electromechanical sensing*. Springer Science & Business Media.
- Tiwari, Santosh K et al. (2016). “Magical allotropes of carbon: prospects and applications”. In: *Critical Reviews in Solid State and Materials Sciences* 41.4, pp. 257–317.

- Huang, Xiao et al. (2011). “Graphene-based materials: synthesis, characterization, properties, and applications”. In: *small* 7.14, pp. 1876–1902.
- Agarwal, Arvind, Debrupa Lahiri, and Srinivasa Rao Bakshi (2018). *Carbon nanotubes: reinforced metal matrix composites*. CRC press.
- Abbott?S, In Edwin (2007). “Graphene: exploring carbon flatland”. In: *Phys. Today* 60.8, p. 35.
- Bolotin, Kirill I et al. (2008). “Ultrahigh electron mobility in suspended graphene”. In: *Solid state communications* 146.9-10, pp. 351–355.
- Geim, AK (2009). “Nature Mater. 6, 183 (2007); AH Castro Neto, F. Guinea, NMR Peres, KS Novoselov, and AK Geim”. In: *Rev. Mod. Phys* 81.1, p. 109.
- Kauling, Alan P et al. (2018). “The worldwide graphene flake production”. In: *Advanced Materials* 30.44, p. 1803784.
- Mortensen, A and J Llorca (2010). “Metal Matrix Composites Annual Review of Materials Research”. In:
- Sidhu, Sarabjeet Singh, Sanjeev Kumar, and Ajay Batish (2016). “Metal matrix composites for thermal management: a review”. In: *Critical Reviews in Solid State and Materials Sciences* 41.2, pp. 132–157.
- Miracle, DB (2005). “Metal matrix composites—from science to technological significance”. In: *Composites science and technology* 65.15-16, pp. 2526–2540.
- Macke, Anthony, BF Schultz, and Pradeep Rohatgi (2012). “Metal matrix composites”. In: *Adv. Mater. Processes* 170.3, pp. 19–23.
- ClyneTW, WithersPJ (1993). *AnIntroductiontoMetalMatrixComposites*.
- Ibrahim, IA, FA Mohamed, and EJ Lavernia (1991). “Particulate reinforced metal matrix composites?a review”. In: *Journal of materials science* 26.5, pp. 1137–1156.
- Chawla, Krishan K (2012). “Metal matrix composites”. In: *Composite materials*. Springer, pp. 197–248.

- Chou, TW, A Kelly, and A Okura (1985). “Fibre-reinforced metal-matrix composites”. In: *Composites* 16.3, pp. 187–206.
- Shirvanimoghaddam, Kamyar et al. (2017). “Carbon fiber reinforced metal matrix composites: Fabrication processes and properties”. In: *Composites Part A: Applied Science and Manufacturing* 92, pp. 70–96.
- Vijayaram, TR et al. (2006). “Fabrication of fiber reinforced metal matrix composites by squeeze casting technology”. In: *Journal of Materials Processing Technology* 178.1-3, pp. 34–38.
- Chawla, Nikhilesh and Y-L Shen (2001). “Mechanical behavior of particle reinforced metal matrix composites”. In: *Advanced engineering materials* 3.6, pp. 357–370.
- Zhang, ZF, LC Zhang, and YW Mai (1995). “Wear of ceramic particle-reinforced metal-matrix composites”. In: *Journal of materials science* 30.8, pp. 1961–1966.
- Wang, Jingyue et al. (2012). “Reinforcement with graphene nanosheets in aluminum matrix composites”. In: *Scripta Materialia* 66.8, pp. 594–597.
- Kumar, HG Prashantha and M Anthony Xavior (2014). “Graphene reinforced metal matrix composite (GRMMC): a review”. In: *Procedia Engineering* 97, pp. 1033–1040.
- HG, Prashantha Kumar and Anthony Xavior (2017). “Tribological aspects of graphene-aluminum nanocomposites”. In: *Graphene Materials-Structure, Properties and Modifications*. IntechOpen.
- Kasar, Ashish K, Guoping Xiong, and Pradeep L Menezes (2018). “Graphene-reinforced metal and polymer matrix composites”. In: *Jom* 70.6, pp. 829–836.
- Nieto, Andy et al. (2017). “Graphene reinforced metal and ceramic matrix composites: a review”. In: *International Materials Reviews* 62.5, pp. 241–302.
- Nautiyal, Hemant et al. (2019). “Copper matrix composites reinforced by rGO-MoS₂ hybrid: Strengthening effect to enhancement of tribological properties”. In: *Composites Part B: Engineering* 173, p. 106931.

- Xiao, Jin-Kun et al. (2017). “Tribological behavior of copper-molybdenum disulfide composites”. In: *Wear* 384, pp. 61–71.
- Takeda, Sho et al. (2017). “Cu-based MoS₂-dispersed composite material formed by the compression shearing method at room temperature”. In: *Tribology Online* 12.2, pp. 29–36.
- Hu, Zengrong et al. (2016b). “Laser sintered graphene nickel nanocomposites”. In: *Journal of Materials Processing Technology* 231, pp. 143–150.
- Zandiataashbar, A, RC Picu, and N Koratkar (2012). “Mechanical behavior of epoxy-graphene platelets nanocomposites”. In: *Journal of engineering materials and technology* 134.3.
- Song, Y et al. (2016). “Microscopic mechanical properties of titanium composites containing multi-layer graphene nanofillers”. In: *Materials & Design* 109, pp. 256–263.
- Chu, Ke and Chengchang Jia (2014). “Enhanced strength in bulk graphene–copper composites”. In: *physica status solidi (a)* 211.1, pp. 184–190.
- Li, Meixia et al. (2014b). “Highly enhanced mechanical properties in Cu matrix composites reinforced with graphene decorated metallic nanoparticles”. In: *Journal of materials science* 49.10, pp. 3725–3731.
- Chu, Ke et al. (2018a). “Anisotropic mechanical properties of graphene/copper composites with aligned graphene”. In: *Materials Science and Engineering: A* 713, pp. 269–277.
- Asgharzadeh, Hamed and Maryam Sedigh (2017). “Synthesis and mechanical properties of Al matrix composites reinforced with few-layer graphene and graphene oxide”. In: *Journal of Alloys and Compounds* 728, pp. 47–62.
- Nieto, Andy, Debrupa Lahiri, and Arvind Agarwal (2012). “Synthesis and properties of bulk graphene nanoplatelets consolidated by spark plasma sintering”. In: *Carbon* 50.11, pp. 4068–4077.

- Pérez-Bustamante, R et al. (2014). “Microstructural and hardness behavior of graphene-nanoplatelets/aluminum composites synthesized by mechanical alloying”. In: *Journal of alloys and compounds* 615, S578–S582.
- Chu, Ke et al. (2018c). “Largely enhanced thermal conductivity of graphene/copper composites with highly aligned graphene network”. In: *Carbon* 127, pp. 102–112.
- Hu, Z et al. (2016a). “Graphene-reinforced metal matrix nanocomposites—a review”. In: *Materials Science and Technology* 32.9, pp. 930–953.
- Kim, WJ, TJ Lee, and SH Han (2014). “Multi-layer graphene/copper composites: Preparation using high-ratio differential speed rolling, microstructure and mechanical properties”. In: *Carbon* 69, pp. 55–65.
- Dutkiewicz, Jan et al. (2015). “Microstructure and properties of bulk copper matrix composites strengthened with various kinds of graphene nanoplatelets”. In: *Materials Science and Engineering: A* 628, pp. 124–134.
- Borkar, Tushar et al. (2015). “Excellent strength–ductility combination in nickel-graphite nanoplatelet (GNP/Ni) nanocomposites”. In: *Journal of Alloys and Compounds* 646, pp. 135–144.
- Yalçın, ED et al. (2019). “Enhancement of wear and corrosion resistance of ZA27/nanographene composites produced by powder metallurgy”. In: *Arabian Journal for Science and Engineering* 44.2, pp. 1437–1445.
- Salvo, C et al. (2019). “Enhanced mechanical and electrical properties of novel graphene reinforced copper matrix composites”. In: *Journal of Alloys and Compounds* 777, pp. 309–316.
- Yue, Hongyan et al. (2017). “Effect of ball-milling and graphene contents on the mechanical properties and fracture mechanisms of graphene nanosheets reinforced copper matrix composites”. In: *Journal of Alloys and Compounds* 691, pp. 755–762.
- Shin, SE et al. (2015). “Strengthening behavior of few-layered graphene/aluminum composites”. In: *Carbon* 82, pp. 143–151.

- Bhaduria, Alok, Lavish K Singh, and Tapas Laha (2019). “Combined strengthening effect of nanocrystalline matrix and graphene nanoplatelet reinforcement on the mechanical properties of spark plasma sintered aluminum based nanocomposites”. In: *Materials Science and Engineering: A* 749, pp. 14–26.
- Chen, Qiwen, Luyan Zhang, and Gang Chen (2012). “Facile preparation of graphene-copper nanoparticle composite by in situ chemical reduction for electrochemical sensing of carbohydrates”. In: *Analytical chemistry* 84.1, pp. 171–178.
- Wang, Lidong et al. (2017). “Graphene-copper composite with micro-layered grains and ultrahigh strength”. In: *Scientific Reports* 7.1, pp. 1–10.
- Li, Xuesong et al. (2009). “Large-area synthesis of high-quality and uniform graphene films on copper foils”. In: *science* 324.5932, pp. 1312–1314.
- Naseer, Abqaat et al. (2019). “A review of processing techniques for graphene-reinforced metal matrix composites”. In: *Materials and Manufacturing Processes* 34.9, pp. 957–985.
- Clyne, TW and PJ Withers (1995). *An introduction to metal matrix composites*. Cambridge university press.
- Hidalgo-Manrique, Paloma et al. (2017). “Microstructure and mechanical behaviour of aluminium matrix composites reinforced with graphene oxide and carbon nanotubes”. In: *Journal of Materials Science* 52.23, pp. 13466–13477.
- Young, Robert J et al. (2018). “The mechanics of reinforcement of polymers by graphene nanoplatelets”. In: *Composites Science and Technology* 154, pp. 110–116.
- Suk, Ji Won et al. (2010). “Mechanical properties of monolayer graphene oxide”. In: *ACS nano* 4.11, pp. 6557–6564.
- Ruiz-Vargas, Carlos S et al. (2011). “Softened elastic response and unzipping in chemical vapor deposition graphene membranes”. In: *Nano letters* 11.6, pp. 2259–2263.
- Nicholl, Ryan JT et al. (2015). “The effect of intrinsic crumpling on the mechanics of free-standing graphene”. In: *Nature communications* 6.1, pp. 1–7.

- Ahmad, SNAS, J Hashim, and MI Ghazali (2007). “Effect of porosity on tensile properties of cast particle reinforced MMC”. In: *Journal of composite materials* 41.5, pp. 575–589.
- Oliver, Warren Carl and George Mathews Pharr (1992). “An improved technique for determining hardness and elastic modulus using load and displacement sensing indentation experiments”. In: *Journal of materials research* 7.6, pp. 1564–1583.
- Xia, Xiaodong et al. (2017). “A unified theory of plasticity, progressive damage and failure in graphene-metal nanocomposites”. In: *International journal of plasticity* 99, pp. 58–80.
- Cao, Huaijie et al. (2019). “Thermal properties of in situ grown graphene reinforced copper matrix laminated composites”. In: *Journal of Alloys and Compounds* 771, pp. 228–237.
- Fu, Kai et al. (2018). “An approach for fabricating Ni@ graphene reinforced nickel matrix composites with enhanced mechanical properties”. In: *Materials Science and Engineering: A* 715, pp. 108–116.
- Chen, Yakun et al. (2016). “Fabrication of in-situ grown graphene reinforced Cu matrix composites”. In: *Scientific reports* 6.1, pp. 1–9.
- Liu, Guang et al. (2017). “In-situ synthesis of graphene decorated with nickel nanoparticles for fabricating reinforced 6061Al matrix composites”. In: *Materials Science and Engineering: A* 699, pp. 185–193.
- Guo, Siyuan et al. (2020). “In situ synthesis of high content graphene nanoplatelets reinforced Cu matrix composites with enhanced thermal conductivity and tensile strength”. In: *Powder Technology* 362, pp. 126–134.
- Kawk, Sae-Rom, Terry A Ring, and Byung-Sang Choi (2019). “A simple two-step fabrication route for Cu composite reinforced by three-dimensional graphene network”. In: *Journal of Industrial and Engineering Chemistry* 70, pp. 484–488.

- Zhang, Xiang et al. (2020). “A powder-metallurgy-based strategy toward three-dimensional graphene-like network for reinforcing copper matrix composites”. In: *Nature communications* 11.1, pp. 1–13.
- Shu, Rui et al. (2019). “Synergetic effect of nano-carbon and HBN on microstructure and mechanical properties of Cu/Ti₃SiC₂/C nanocomposites”. In: *Materials Science and Engineering: A* 755, pp. 128–137.
- Li, Mei-Xia et al. (2015b). “Reduced graphene oxide dispersed in copper matrix composites: Facile preparation and enhanced mechanical properties”. In: *physica status solidi (a)* 212.10, pp. 2154–2161.
- Jo, Yongdeok et al. (2019). “Tensile properties of three-dimensionally interconnected graphene-networked Cu composite and changes in its microstructure in relation to heat treatment temperature”. In:
- Tang, Yanxia et al. (2014). “Enhancement of the mechanical properties of graphene–copper composites with graphene–nickel hybrids”. In: *Materials Science and Engineering: A* 599, pp. 247–254.
- Cui, Ye et al. (2014). “Effect of ball milling on the defeat of few-layer graphene and properties of copper matrix composites”. In: *Acta Metallurgica Sinica (English Letters)* 27.5, pp. 937–943.
- Chu, Ke et al. (2018b). “Interface structure and strengthening behavior of graphene/CuCr composites”. In: *Carbon* 133, pp. 127–139.
- Kim, Youbin et al. (2013). “Strengthening effect of single-atomic-layer graphene in metal–graphene nanolayered composites”. In: *Nature communications* 4.1, pp. 1–7.
- Kato, Masaharu (2014). “Hall–Petch relationship and dislocation model for deformation of ultrafine-grained and nanocrystalline metals”. In: *Materials Transactions* 55.1, pp. 19–24.

- Zhang, Xiang et al. (2017b). “Achieving high strength and high ductility in metal matrix composites reinforced with a discontinuous three-dimensional graphene-like network”. In: *Nanoscale* 9.33, pp. 11929–11938.
- Li, Xue, Terry Arthur Ring, and Byung-Sang Choi (2019). “Thermal Conductivity of Three-Dimensionally Interconnected Graphene-Networked Cu Composite Fabricated by a Simple Two-Step Process”. In: *Korean Journal of Metals and Materials* 57.8, pp. 529–534.
- Mahvash, F et al. (2017). “Corrosion resistance of monolayer hexagonal boron nitride on copper”. In: *Scientific reports* 7.1, pp. 1–5.
- Bartolucci, Stephen F et al. (2011). “Graphene–aluminum nanocomposites”. In: *Materials Science and Engineering: A* 528.27, pp. 7933–7937.
- Yang, Wenshu et al. (2018). “Microstructure and mechanical properties of graphene nanoplates reinforced pure Al matrix composites prepared by pressure infiltration method”. In: *Journal of Alloys and Compounds* 732, pp. 748–758.
- Singh, Sikander Pal, RS Joshi, and VK Singla (2018). “Effect of Hexa Boron Nitride and REO Addition on Wear and Corrosion Behavior of Hard-Facing on Mild Steel”. PhD thesis.
- Elkady, Omayma AM et al. (2015). “Physico-mechanical and tribological properties of Cu/h-BN nanocomposites synthesized by PM route”. In: *Journal of Alloys and Compounds* 625, pp. 309–317.
- Liu, Zheng et al. (2013). “Ultrathin high-temperature oxidation-resistant coatings of hexagonal boron nitride”. In: *Nature communications* 4.1, pp. 1–8.
- Duan, Xiaoming et al. (2016). “Review on the properties of hexagonal boron nitride matrix composite ceramics”. In: *Journal of the European Ceramic Society* 36.15, pp. 3725–3737.

- Kim, Seong-Eun and In-Jin Shon (2018). “Rapid sintering of nanocrystalline (W, Ti) C-graphene composites”. In: *Journal of the Korean Institute of Metals and Materials* 56.12, pp. 854–860.
- Song, Myoung Youp, Young Jun Kwak, and Eunho Choi (2018). “Hydrogen storage properties of Mg-graphene composites”. In: *Korean Journal of Metals and Materials* 56.7, pp. 524–531.
- Wu, Mingliang et al. (2019). “High oxidation resistance of CVD graphene-reinforced copper matrix composites”. In: *Nanomaterials* 9.4, p. 498.
- Tripathi, Khagendra, Gobinda Gyawali, and Soo Wohn Lee (2017). “Graphene coating via chemical vapor deposition for improving friction and wear of gray cast iron at interfaces”. In: *ACS applied materials & interfaces* 9.37, pp. 32336–32351.
- Gopinath, S, M Prince, and GR Raghav (2020). “Enhancing the mechanical, wear and corrosion behaviour of stir casted aluminium 6061 hybrid composites through the incorporation of boron nitride and aluminium oxide particles”. In: *Materials Research Express* 7.1, p. 016582.
- Reddy, A Chennakesava (2013). “Study of factors influencing sliding wear behavior of hexagonal boron nitride reinforced AA6061 metal matrix composites”. In: *5th International Conference on Modern Materials and Manufacturing, Bangalore*, pp. 409–413.
- Zitoun, Essa and A Chennakesava Reddy (2008). “Microstructure-Property Relationship of AA3003/Boron Nitride Particle-Reinforced Metal Matrix Composites Cast by Bottom-Up Pouring”. In: *6th National Conference on Materials and Manufacturing Processes, Hyderabad*, pp. 115–119.
- Khatavkar, Mr Rushikesh A et al. (2018). “Influence of Hexagonal Boron Nitride on Tribological Properties of AA2024-hBN Metal Matrix Composite”. In: *Int. Res. J. Eng. Technol.* 5.5.

- Cho, Woo-Jin and In-Jin Shon (2018). “Effect of BN addition on the mechanical properties of TiN-BN composites”. In: *Korean Journal of Metals and Materials* 56.9, pp. 658–663.
- El-Tantawy, Ahmed, Walid M Daoush, and Ahmed E El-Nikhaily (2018). “Microstructure and properties of BN/Ni-Cu composites fabricated by powder technology”. In: *Journal of Experimental Nanoscience* 13.1, pp. 174–187.
- Li, J.L. et al. (2015a). “Microstructure and tensile properties of bulk nanostructured aluminum/graphene composites prepared via cryomilling”. In: *Materials Science and Engineering: A* 626, pp. 400–405. ISSN: 0921-5093. DOI: <https://doi.org/10.1016/j.msea.2014.12.102>. URL: <https://www.sciencedirect.com/science/article/pii/S092150931401613X>.
- Cao, Mu et al. (2017). “Aligning graphene in bulk copper: Nacre-inspired nanolaminated architecture coupled with in-situ processing for enhanced mechanical properties and high electrical conductivity”. In: *Carbon* 117, pp. 65–74.
- Jiang, Rongrong et al. (2016). “Copper-graphene bulk composites with homogeneous graphene dispersion and enhanced mechanical properties”. In: *Materials Science and Engineering: A* 654, pp. 124–130.
- Wang, Miao et al. (2019). “Direct synthesis of high-quality graphene on Cu powders from adsorption of small aromatic hydrocarbons: a route to high strength and electrical conductivity for graphene/Cu composite”. In: *Journal of Alloys and Compounds* 798, pp. 403–413.
- Gautam, Chandkiram et al. (2018). “Synthesis and 3D interconnected nanostructured h-BN-based biocomposites by low-temperature plasma sintering: bone regeneration applications”. In: *ACS omega* 3.6, pp. 6013–6021.
- Guiney, Linda M et al. (2018). “Three-dimensional printing of cytocompatible, thermally conductive hexagonal boron nitride nanocomposites”. In: *Nano letters* 18.6, pp. 3488–3493.

- Yin, Jun et al. (2013). “Ultralight three-dimensional boron nitride foam with ultralow permittivity and superelasticity”. In: *Nano letters* 13.7, pp. 3232–3236.
- Chatterjee, Shahana et al. (2012). “Syntheses of boron nitride nanotubes from borazine and decaborane molecular precursors by catalytic chemical vapor deposition with a floating nickel catalyst”. In: *Chemistry of Materials* 24.15, pp. 2872–2879.
- Ding, Yanhuai et al. (2017). “Mechanical Properties of GO Nanostructures Prepared from Freeze-Drying Method”. In: *Novel Nanomaterials-Synthesis and Applications*. IntechOpen.
- German, Randall M (2010). “Coarsening in sintering: grain shape distribution, grain size distribution, and grain growth kinetics in solid-pore systems”. In: *Critical reviews in solid state and materials sciences* 35.4, pp. 263–305.
- McDonald, SA et al. (2017). “Microstructural evolution during sintering of copper particles studied by laboratory diffraction contrast tomography (LabDCT)”. In: *Scientific Reports* 7.1, pp. 1–11.
- Joshi, Sushobhan et al. (2012). “Boron nitride on Cu (111): an electronically corrugated monolayer”. In: *Nano letters* 12.11, pp. 5821–5828.
- Khan, Aamar F et al. (2017). “2D hexagonal boron nitride (2D-hBN) explored as a potential electrocatalyst for the oxygen reduction reaction”. In: *Electroanalysis* 29.2, pp. 622–634.
- Koepke, Justin C et al. (2016). “Role of pressure in the growth of hexagonal boron nitride thin films from ammonia-borane”. In: *Chemistry of Materials* 28.12, pp. 4169–4179.

APPENDIX A: Main Reagents and Materials

The reagents and materials used in this work and their origin are listed in Table A.1

Table A.1: Main Reagents and Materials.

| Reagents and materials | Quality |
|---|---|
| Copper powder | 99% purity, 14-25 μm (spherical) |
| Nickel powder | 99.5% purity, 1~5 μm (spherical) |
| Hydrochloric acid | Assay above 35% , extra pure |
| $\text{FeCl}_3 \cdot 6\text{H}_2\text{O}$ | 97.0-102.0% |
| Ethanol | 99.5% purity |
| Acetone | 99.5% purity |

APPENDIX B: Synthesis and Characterization Tools

B.1 CVD System

The CVD system mainly consists of quartz tube furnace, gas flow meters, gas pressure controller and rotary pump. CVD furnace has following specifications.

1. Automatic nickel-chromium thermocouple which can control temperature up to 1100°C.
2. Quartz tube in the furnace has 80 mm diameter and 1500 mm length. Temperature is controlled by three thermocouples.
3. Quartz jig where samples are placed.

B.1.1 Pneumatic Control and Vacuum System

As a device for preparing composite materials by CVD method, its gas path system, flow meter and vacuum degree control system has a significant impact on the quality of the prepared graphene material. Among them, all digital flowmeters are calibrated with nitrogen (N₂), the error rate is full the range is $\pm 1.5\%$ to ensure the accuracy of each reaction gas flow rate during the entire experiment. The overall structure of the gas circuit is connected by welded technology to ensure air tightness. A total of 3 gases including argon (Ar, 99.999%), Hydrogen (H₂, 99.999%) and methane (CH₄, 99.995%) are designed to control the experiment conditions. The vacuum system consists of a first-stage diaphragm pump and a second-stage turbine and the ultimate vacuum can reach 1×10^{-8} mbar.

B.2 Other Experimental Instruments

Table B.1 shows the other experimental instruments and their usage

Table B.1: Instruments and their usage.

| Instrument | Model | Usage |
|---------------------|--------------------------------------|--|
| Ultrasonic cleaner | BRANSON 2210R-DTH | Washing and cleaning |
| Drying oven | HANBAEK SCIENTIFIC CO.,LTD (HB-501M) | Drying |
| Vacuum glove box | JISICO J-924 AHO | Protection against moisture and oxidation |
| Polishing machine | ALLIED TWINPREP 3 7M | Surface polishing to reveal microstructure |
| Analytical Balances | SHINKO DENSHICO.,LTD (AF-R220E-D) | Weight the samples |

B.3 Characterization Methods

Different instruments were employed in this study to characterize the materials fabricated and trace the reactions during the synthesis processes and are given in Table B.2. This section mainly introduces the graphene/hBN material structure characterization technology used in this work, and the material structure and the specific method characteristics of various physical properties are described in detail. These tools helped to optimize the synthesis conditions of the composites.

Table B.2: Instruments and their usage.

| Instrument | Model |
|------------|--------------------|
| OM | NIKON |
| XRD | PANalytical CubiX3 |
| SEM | HITACHI S-4800 |
| TEM | TECNAI G20FEI |